



The issue of stress state during mechanical tests to assess cladding performance during a reactivity-initiated accident (RIA)

J. Desquines^{a,*}, D.A. Koss^b, A.T. Motta^b, B. Cazalis^a, M. Petit^a

^aIRSN, DPAM, 13115 Saint-Paul-lez-Durance Cedex, France

^bThe Pennsylvania State University, 227 Reber Building, University Park, PA 16802, USA

ARTICLE INFO

Article history:

Received 27 July 2010

Accepted 9 March 2011

Available online 7 April 2011

ABSTRACT

The mechanical test procedures that address fuel cladding failure during a RIA are reviewed with an emphasis on the development of test procedures that determine the deformation and fracture behavior of cladding under conditions similar to those reached in a RIA. An analysis of cladding strain data from experimental research reactor test programs that have simulated the RIA is presented. These data show that the cladding undergoes deformation characterized by hoop extension subject to a range of multiaxial stress states and strain paths comprised between plane-strain (no axial extension of the cladding tube) and equal-biaxial tension (equal strain in both the hoop and the axial orientations). Current mechanical test procedures of cladding material are then reviewed with a focus on their ability to generate the appropriate deformation response and to induce the prototypical multiaxial stress states and failure modes activated during a RIA. Two main groups of tests currently exist. In the first group, the deformation behavior of the cladding is examined by several variations of hoop tensile tests in which an axial contraction of the specimen gage section occurs such that a near-uniaxial tension stress state results; finite element analyses are then usually employed to deduce the deformation response, often under conditions of an assumed coefficient of friction between the specimen and test fixtures. The second group includes test procedures which attempt to reproduce the deformation and failure conditions close to those seen during a RIA such that any stress-state corrections of the failure conditions are comparatively small. The advantages and disadvantages of all of these deformation/fracture tests are discussed with special reference to testing high burnup fuel cladding.

© 2011 Elsevier B.V. All rights reserved.

1. Introduction

Both the loading path and the loading mode are critical factors in determining the failure of a structural metal component. As a result, a failure criterion needs to take into account the applied stress state or (if ductile) the strain-path history of the component during failure. The development of such a failure criterion relies in turn on an experimental data base that addresses the sensitivity of the failure process to an appropriate range of stress states and strain paths. In the case of a postulated RIA in pressurized light water nuclear power reactors, the thin-wall zirconium alloy fuel cladding tubes may be subjected to Pellet–Cladding–Mechanical Interaction (PCMI) which imposes a range of stress states on the cladding as it deforms, depending on the friction coefficient or the degree of bonding between the cladding and the pellet. Predicting cladding failure under such conditions must take into account not only the material state of the cladding (i.e., fuel burnup issues such as

the level of irradiation and hydrogen content/distribution/alignment) but also the imposed thermal/mechanical conditions of temperature, strain rate, and (importantly) stress state. The mode of loading, displacement-controlled loading for PCMI and potentially load-controlled inner pressure loading at higher fuel temperature, is also important for an accurate prediction of cladding failure. The present paper addresses the development of mechanical test procedures that examine the influence of stress state on the failure behavior of fuel cladding in general and specifically during a reactivity-initiated accident.

A RIA may be caused by a control rod ejection or drop, inducing a near-instantaneous increase in reactivity in the nearby fuel rods. As a result of this reactivity insertion, the fission rate increases exponentially until the effect of Doppler broadening stops the chain reaction. The energy deposited in the fuel during the reactivity excursion causes the temperature of the fuel to increase, which in turn causes the fuel to expand and impinge on the cladding. Because this excursion is very fast, the cladding may still remain close to its nominal temperature when the fuel impacts it. If the cladding has become embrittled during reactor operation, it can fail during such a transient. The possibility of such an accident has been recognized previously, and tests were conducted that

* Corresponding author. Address: IRSN, DPAM/SEREM, Bâtiment 327, 13115 Saint-Paul-lez-Durance Cedex, France. Tel.: +33 04 42 19 94 90; fax: +33 04 42 19 91 62.

E-mail address: jean.desquines@irsn.fr (J. Desquines).

led to the establishment of enthalpy limits to avoid fuel failure during a RIA [1]. Recently, it has been shown that such limits may be degraded by long term exposure of the fuel cladding to the reactor environment, causing radiation damage and hydriding [2]. As a result, significant work has been performed to reassess RIA limits at high fuel burnup [3–15].

When submitted to PCMI loading during a RIA event, the cladding deforms under a biaxial stress state such that while the hoop stress ($\sigma_{\theta\theta}$) is the maximum component of the stress tensor in the cladding, a large axial tensile stress (σ_{zz}) is also applied. Thus the cladding is constrained to deform under a degree of stress biaxiality that can range from $(\sigma_{zz}/\sigma_{\theta\theta}) \approx 0.5\text{--}1.0$, depending on the fuel-cladding contact conditions, as described below. These stress states imply that the relevant strain paths range from roughly plane-strain tension to equal-biaxial tension – which is quite different from the uniaxial tensile path commonly applied in many studies. It has also been shown previously that the stress state can be influential in the failure of hydrided Zircaloy with influence depending on the considered study [16,18]. Thus, in order to predict accurately the failure of cladding under RIA conditions, knowledge of its deformation/fracture behavior under multiaxial tension conditions is critical.

Most studies conducted to characterize the mechanical properties of irradiated cladding, have been performed under uniaxial stress conditions with the loading direction aligned either along the tube axis or along the transverse hoop orientation. For example, ring samples have recently been loaded with inserted mandrels in order to obtain displacement-controlled loading in the hoop direction [12]. The samples used in these studies consist of axially short rings machined from fuel claddings, for which the resulting strain path is uniaxial tension, as discussed below. While the resulting behavior can be used to check the extent of cladding ductility or embrittlement after in-pile irradiation, it does not provide an accurate basis for predicting cladding failure strains under multiaxial stress states encountered during a RIA event. Tube burst testing has also been performed on irradiated cladding. While a multiaxial (near plane-strain) stress state is initially imposed in such tests during uniform deformation, failure is very sensitive to local imperfections, resulting in low estimates of the far-field fracture strain. After significant strain accumulation during the pressurization of close ended specimens, the local stress/strain state and strain rates are usually not well established. For these reasons, several experimental studies based on innovative testing concepts have recently been performed to address the issue of cladding failure under multiaxial stress states. The aim of the present study is to review recent developments in experimental procedures that address cladding failure behavior under multiaxial stress states in general and specifically under stress states encountered during a RIA event.

2. Background: cladding loading during RIA transients

The relevance of experimental test data to cladding failure during a RIA event depends significantly on the relationship of those data (and the related analyses) to the multiaxial stress states/strain paths encountered by the cladding during the transient.

2.1. The RIA transient

In a RIA, a rod ejection or drop causes a sudden increase in fission rate in the fuel, which is eventually turned around by the Doppler effect, resulting in a pulse, which has a full width half maximum which can be as small as tens of milliseconds. The pulse deposits energy in the fuel and causes the fuel temperature to increase. Consequently, the fuel swells and can impact the cladding.

Because the energy deposition is so fast, the cladding temperature may not have increased by the time the fuel impacts it, and thus the cladding mechanical response may be governed by the initial cladding temperature at the start of the transient. This is the *low temperature* phase of the transient, also called the PCMI phase. In the PCMI phase, even as the fuel temperature increases the cladding remains at a temperature close to the coolant temperature. If the cladding survives this phase (tens of milliseconds), its temperature increases along with the coolant temperature. This increase in heat flux can cause the coolant to go through departure from nucleate boiling (DNB) during which a blanket of steam is formed at the cladding surface, which in turn reduces the heat transfer and can cause further increases of temperature. The temperature increase also causes the yield stress to decrease, and can cause cladding failure by ballooning driven by the internal cladding pressure from fission gas release. This is the *high temperature* phase of the transient. RIA testing aims to reproduce the conditions and test cladding failure limits at one of the two phases. It should be recognized that DNB does not occur in liquid metal cooled reactors (such as in the CABRI REP-Na program) since sodium boiling cannot be achieved; in this case the PCMI phase ends by exhaustion of thermal dilation of the fuel in the absence of fuel fusion (see REP-Na 2 test [4] for example).

2.1.1. High and low burnup fuel

It is of interest to test both high and low burnup fuel, and some significant differences exist between the two. At low burnup, a gap can exist between the fuel and the cladding, which progressively closes with increasing burnup. At high burnups, the uranium dioxide and zirconium interact, such that the fuel pellet and the zirconium alloy cladding become effectively bonded [19,20]. Although the level of radiation damage and associated mechanical property changes largely saturate at relatively low burnup, the amount of hydrogen in the material gradually increases with burnup, and the distribution of such hydrogen also evolves in response to temperature and stress gradients in the cladding. At high burnups, a hydride rim can form on the outer part of the cladding surface and in case of oxide spalling, hydride blisters can form. Both blisters and rims can serve as initiation points for failure during RIA transients. The final significant difference with burnup level is the amount of fission gas produced and its distribution in the fuel. Low burnup fuel has limited fission gas content and the few fission gas bubbles are confined within the fuel grains. Clearly the amount of fission gas contained in the fuel rod increases with burnup, such that the internal pressure is higher at high burnup and more gas is available for release during the transient. Finally, in high burnup fuel several processes modify the fuel structure, including fuel cracking, fission gas release, and the formation of the rim structure at the outer surface of the pellet as a consequence of self-shielding leading to higher plutonium concentration at the fuel rim. The higher concentration of plutonium causes an increase in the fission rate in the rim relatively to the middle of the pellet, which in turn creates a structure consisting of small grains, and a high density of fission gas bubbles [21].

2.1.2. RIA cladding response

The cladding response during those two phases at low and high burnup is different. When subjecting high burnup fuel to RIA transients, the gap is already closed and indeed the fuel and cladding may be bonded, so PCMI loading occurs right away. As discussed below, the clad-fuel bonding causes a more equal biaxial cladding loading. Embrittlement due to previous hydrogen ingress can cause the cladding to fail during the PCMI period. The PCMI loading phase ends when the cladding temperature is high enough to dissolve the hydrogen and significantly increase ductility. As the cladding temperature increases large fission gas release occurs from

the fuel. During the high temperature phase the cladding response is strongly dependent on filling gas pressure at low burnup, and on fission gas pressure at high burnup. The high injected energy temperature increase facilitates the release of fission gas, first from bubbles located at grain boundaries and pores, and then for higher injected energies from fission gas bubbles located within the fuel grains. However, due to the limited fission gas content at low burnup, the fission gases are not expected to contribute directly to cladding failure. At low burnups, cladding failure is more likely to occur by exceeding a temperature and time period that induces transient oxidation of the cladding and consequent embrittlement. Cladding failure is achieved at injected energies exceeding about 200 calories per fuel grams. These results addressing low burnup fuel were mainly established based on SPERT test results [1].

The large amount of fission gas at high burnup can drastically modify the consequences of the post-DNB phase. During this phase, the high burnup fuel rim remains more or less in a sticking contact with the cladding, and macro-porosity forms between the cladding with sticking fuel rim and the remaining part of the fuel. The transition from PCMI loading to gas (filling gas and released fission gas) controlled loading (post-DNB loading) is complex. Gas loading can be applied to the inner wall of the cladding through fuel particles. Grain boundary separation generate complex path for gas and it is usually extremely difficult to determine the loading mode based solely on post-test metallography unless cladding deformation is large. During the post-DNB phase of the NSRR TK-1 [22] test, with significant fission gas release, gas loading was applied to the cladding through a fragmented fuel crown, most of the released gas remained in an axisymmetric free volume formed between the high burnup fuel sticking to the cladding and the rest of the fuel. For this NSRR TK-1 test, large cladding deformation was achieved and the post-test metallography showed large spacing between fuel fragments sticking to the cladding that could not be filled only by the fuel thermal dilatation, thus evidence of gas loading is achieved after this test. The post-DNB phase can prevent PCMI failure by increasing the cladding temperature and consequently increasing cladding ductility, but the consequence of the rapid temperature change are still not very well understood. As a result of the internal gas loading, the post-DNB loading leads to a state of stress of plane-strain deformation (see Table 1).

In the other extreme, when fuel-cladding bonding is perfect, a state of stress of equal biaxial loading occurs as the cladding expands in concert with the fuel. A RIA test surviving the PCMI phase and subjected to a post-DNB phase will experience a strain-path change but retain a memory of the PCMI phase. Thus, some permanent axial extension is expected after the RIA test. The post-DNB phase still needs in-depth further study to achieve a detailed understanding of all the phenomena activated during this phase.

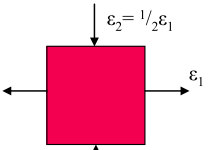
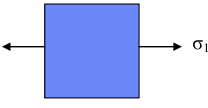
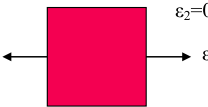
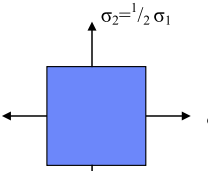
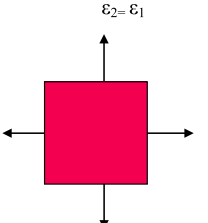
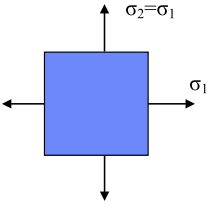
As a result of the above described behavior, the state of stress during RIA loading may involve a strain-path change and can eventually lie somewhere between plane-strain tension and equal-biaxial tension. Table 1 illustrates the states of stress discussed above assuming isotropic plasticity. It should be obvious that both plane-strain tension and equal-biaxial tension are quite different from uniaxial tension. Importantly as will be discussed below, there is evidence that the greater stress biaxiality in either of these types of loading may contribute to lower cladding failure limits relative to uniaxial tension [16,18]. Consequently, unless well established corrective factors are available, the use of uniaxial mechanical testing to predict RIA behavior is likely to be *non conservative*.

2.1.3. The RIA stress state

As will be explained in the following, a fundamental basis for this discussion is that the stress states imposed on the cladding

Table 1

States of stress relevant to the mechanical testing for RIA (assuming isotropic plasticity).

State of stress	Strain	Stress
Uniaxial tension		
Plane-strain tension		
Equal-biaxial tension		

are directly affected by Pellet–Cladding–Mechanical Interaction as influenced by the degree of pellet–cladding bonding. The degree of interaction between the pellet and the cladding, the fission gas release, and the internal gas content directly affects the stress state of the deforming cladding. It is difficult to predict precisely the degree of stress biaxiality (and its strain/time-dependence) within the cladding under RIA conditions, but it can be estimated post mortem as discussed below.

2.2. RIA testing

As mentioned above, three types of tests can be conducted to evaluate cladding mechanical behavior at high fuel burnup: (i) integral tests as well as (ii) tests on defueled irradiated cladding and (iii) separate effects tests performed on non-irradiated artificially hydrided material. The latter two are “separate effects” tests, but the samples in (ii) have in principle the exact microstructure degradation obtained during reactor exposure.

The term “integral tests” refers to tests in which an actual instrumented fuel rod or refabricated “rodlet” is subjected to an actual reactivity insertion event, simulating that which could occur in a reactor. Some of these tests were conducted in the SPERT and PBF facilities in the US and helped set the limits for energy deposition during a RIA [1]. More recent tests have been conducted in the CABRI facility in France, the NSRR facility in Japan and the BGR facility in Russia [5,13,14]. Because of the constraints of working with highly radioactive material, and the specialized instrumentation required, such tests are quite expensive and consequently limited in number.

Testing irradiated cladding is a complementary and simplified way to investigate the mechanical behavior of irradiated cladding. In this case, defueled cladding is tested in a hot cell after reactor exposure, such that the sample will have both hydriding and radiation damage. Since no fuel is involved, the levels of radioactivity are much lower than in integral tests, and it is possible to design test specimens and loading apparatus such that particular testing conditions are satisfied. In this way, the separate effects of various

parameters such as strain rate, stress state, and temperature can be investigated systematically. Programs such as the French testing program PROMETRA [12] have used this approach and have generated much useful data.

Finally, separate effects tests are those in which non-irradiated material is used [23]. They are based on the assumption that hydriding is the main contributor to degradation of ductility in reactor. Thus, by hydrogen charging specimens in a controlled manner and creating well designed specimens, it is possible to investigate in detail and isolate the specific roles of hydride content, orientation, and distribution on failure for a material subjected to particular loading conditions. These tests performed on fresh cladding material can be much more easily performed and allows investigation of the separate effects. The results need then to be related to in-reactor behavior.

2.3. Integral RIA tests

The most reliable assessment of the loading conditions comes from the experimental measurements of the residual strain components, ϵ_{zz} and $\epsilon_{\theta\theta}$, from cladding deformed under simulated RIA tests; (here, ϵ_{zz} and $\epsilon_{\theta\theta}$ are the axial and hoop strain components, respectively).

Two main programs of integral RIA tests have been performed in which the residual strain components have been determined such that multiaxial stress states can be assessed:

- the CABRI RIA tests with sinusoidal axial power profile along the cladding length [4],
- the NSRR RIA tests with flat axial power profile [24].

In measuring post test strains, particular characteristics of each reactor should be mentioned. For the NSRR tests, the ratio of axial to hoop plastic strain ($\epsilon_{zz}/\epsilon_{\theta\theta}$) is uniform along the axial length of the fissile column. For these tests, the plastic strains in hoop direction and axial direction have been obtained by direct measurements of post-test diameter and axial length. For the CABRI tests, the axial distribution of residual hoop strains is non-uniform, taking the form of a sine curve with the maximum residual strain-values near the center of the cladding tube length. The final measured elongation over the length of the CABRI rodlets thus provides post-test axial residual strains on an axially averaged basis, while measurements of the rodlet diameter at several azimuthal locations along its length provide average hoop strain values as a function of location.

Table 2 summarizes the average strain measurements experimentally determined from RIA tests. The CABRI test deformations were averaged along the axial length of the tube that was subjected to RIA loading. These data can be expressed in the form of Fig. 1, which shows the evolution of the strain ratio ($\epsilon_{zz}/\epsilon_{\theta\theta}$) as a

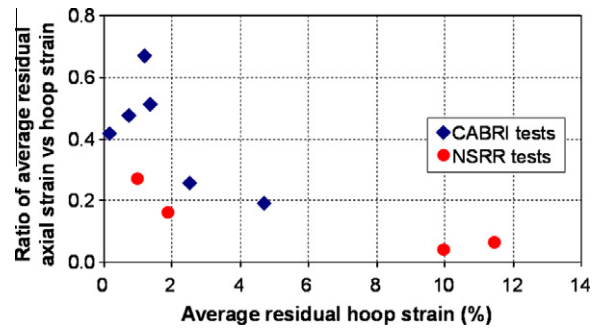


Fig. 1. The strain ratio ($\epsilon_{zz}/\epsilon_{\theta\theta}$) as a function of the average hoop strain ($\epsilon_{\theta\theta}$) for the NSRR and CABRI RIA tests.

function of the hoop strain ($\epsilon_{\theta\theta}$). As might be expected from the previous discussion, the strain ratio varies from a maximum of near equal-biaxial tension when $\epsilon_{zz}/\epsilon_{\theta\theta} = 0.7$ to a near plane-strain condition when $\epsilon_{zz}/\epsilon_{\theta\theta} = 0.0$, the latter occurring when nearly all the deformation is confined to hoop extension. Specifically, the strain ratio conforms to an expected trend: the near plane-strain condition ($\epsilon_{zz}/\epsilon_{\theta\theta} \approx 0.0$) corresponds to two NSRR tests that occurred under high injected energy conditions in stagnant water, consistent with force loading due to internal pressure development after the departure from nucleate boiling (DNB) condition has been reached and the sample is blanketed in vapor and thus at high temperature. Under this condition, the cladding undergoes comparatively large hoop expansion at elevated temperatures when it is relatively soft.

In contrast, the CABRI REP-Na tests, which use liquid sodium as coolant, cause the PCMI to have a greater role in the test up to high injected energies. Because sodium DNB has never been reached during the CABRI REP-Na tests in CABRI facility, the cladding temperature during the REP-Na tests remained low when compared to NSRR tests, performed with water coolant. Thus fission-gas controlled loading is promoted in the NSRR tests because of the higher clad temperature (and consequently lower yield stress) at similar deposited enthalpy.

Taken together, the NSRR and CABRI tests show a distinct strain-path trend in that, when confined to small residual hoop strains, the cladding deformation tends toward equal-biaxial tension ($\epsilon_{zz}/\epsilon_{\theta\theta} \approx 1.0$). In contrast, when cladding has experienced a large degree of hoop extension, the cumulative strain path is near plane-strain tension ($\epsilon_{zz}/\epsilon_{\theta\theta} \approx 0.0$). These test data raise the possibility that at very small strains near yielding, initial cladding deformation occurs under equal-biaxial tension ($\epsilon_{zz}/\epsilon_{\theta\theta} = 1.0$), and then it undergoes a strain-path change to purely plane-strain tension ($\epsilon_{zz}/\epsilon_{\theta\theta} = 0.0$) as gas pressure loading dominates deformation at larger strains/longer times of loading. The cumulative effect would be an eventual “near plane-strain” deformation.

The associated multiaxial stress states may be interpolated from the experimental residual strain data if we consider that the only two non-negligible stress components are the hoop and axial stresses in thin-wall cladding deforming under the von Mises flow rule (assuming isotropic plasticity) and under a condition of plane stress.

Neglecting the radial stress component, the stress tensor is:
$$\bar{\sigma} = \begin{pmatrix} \approx 0 & & \\ & \sigma_{\theta\theta} & \\ & & \sigma_{zz} \end{pmatrix}_{(r,\theta,z)}$$
 and assuming a Von Mises yield criterion, the flow rule indicates that the plastic strain increment is proportional to the deviatoric part of the stress tensor: $\bar{\epsilon}^p = \lambda \cdot dev(\bar{\sigma})$. The ratio of plastic strain rates only depend on the ratio of the stress components:

Table 2 Experimental values of average residual strains from several RIA tests ([13,24–27]).

Test reactor	Test ID #	Average residual strains		
		$\epsilon_{\theta\theta}$ (%)	ϵ_{zz} (%)	$\epsilon_{zz}/\epsilon_{\theta\theta}$
CABRI	RepNa2	1.36	0.69	0.51
CABRI	RepNa3	1.19	0.79	0.67
CABRI	RepNa4	0.17	0.07	0.42
CABRI	RepNa5	0.74	0.35	0.48
CABRI	RepNa6	2.5	0.64	0.26
CABRI	RepNa9	4.7	0.89	0.19
NSRR	HBO-3	1	0.4	0.26
NSRR	TK-1	10	0.92	0.04
NSRR	TK-6	11.5	0.92	0.06
NSRR	ATR-3	1.9	0.3	0.16

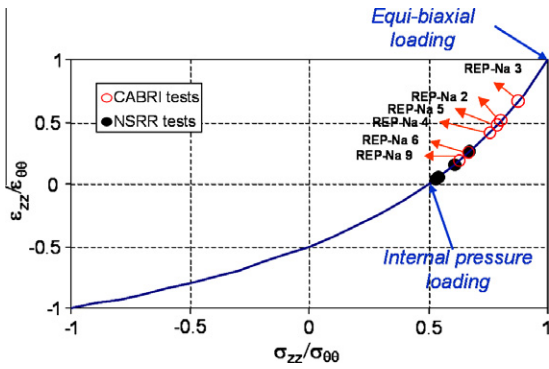


Fig. 2. The strain ratio ($\epsilon_{zz}/\epsilon_{\theta\theta}$) as a function of the stress ratio ($\sigma_{zz}/\sigma_{\theta\theta}$) for a series of RIA tests conducted at the NSRR and CABRI facilities.

$$\begin{pmatrix} \dot{\epsilon}_{rr}^p \\ \dot{\epsilon}_{\theta\theta}^p \\ \dot{\epsilon}_{zz}^p \end{pmatrix}_{(r,\theta,z)} = \frac{\lambda}{3} \begin{pmatrix} -\sigma_{\theta\theta} - \sigma_{zz} & & \\ & 2\sigma_{\theta\theta} - \sigma_{zz} & \\ & & 2\sigma_{zz} - \sigma_{\theta\theta} \end{pmatrix}_{(r,\theta,z)}$$

Assuming a proportional loading (linearly increasing with time), which is a questionable but useful assumption, a simple link between plastic residual strains and biaxial stress state during the RIA can then be established:

$$\frac{\epsilon_{zz}^p}{\epsilon_{\theta\theta}^p} = \frac{2\frac{\sigma_{zz}}{\sigma_{\theta\theta}} - 1}{2 - \frac{\sigma_{zz}}{\sigma_{\theta\theta}}} \quad \text{or inversely} \quad \frac{\sigma_{zz}}{\sigma_{\theta\theta}} = \frac{2\frac{\epsilon_{zz}^p}{\epsilon_{\theta\theta}^p} + 1}{2 + \frac{\epsilon_{zz}^p}{\epsilon_{\theta\theta}^p}} \quad (1)$$

where σ_{zz} and $\sigma_{\theta\theta}$ are the corresponding axial and hoop stress components, respectively.

Eq. (1) may be used in order to determine the stress ratio based on post-test residual strain measurements such as was done in Table 2. It is interesting to mention that, in the absence of PCMI, the internal pressure loading conditions of cladding with end caps induce a stress ratio of 0.5, which corresponds to a zero strain ratio, in other words a plane-strain condition.

Assuming Eq. (1) for the RIA tests in Table 2, Fig. 2 shows the strain ratio $\epsilon_{zz}/\epsilon_{\theta\theta}$ as a function of the biaxial stress ratio $\sigma_{zz}/\sigma_{\theta\theta}$ with individual tests as data points and the curve represented by Eq. (1) plotted as a solid line. Fig. 2 reveals the large degree of multiaxiality of the stress state, the axial stress σ_{zz} ranging from 0.5 $\sigma_{\theta\theta}$ to 0.9 $\sigma_{\theta\theta}$, and it shows that Eq. (1) predicts well the strain ratio.

In summary, these integral test data as well as our understanding of the conditions under which the cladding deforms during a RIA indicate the high degree of the multiaxiality of the stress states that characterize cladding behavior under RIA conditions. Given the sensitivity of material failure to stress state and strain paths, there is a clear need to establish the relationship between the stress states imposed during the mechanical testing and those, encountered during a RIA, that limit cladding performance under RIA conditions. Ideally, the test conditions should explore a range of multiaxial stress states such as those illustrated in Fig. 2, perhaps in the form of a “failure map” linking failure strains to stress state. The alternative is to rely on an analysis that uses a failure criterion that accurately takes into account the influence of stress state on failure such that simple experimental data at a given stress state can be used to predict failure under the complex conditions imposed during a RIA.

3. The influence of multiaxiality on cladding failure conditions

3.1. The influence of stress state and hydrogen: uniform hydrides and failure due to damage accumulation

An experimental study from Yunchang and Koss [16] initially highlighted the influence of loading multiaxiality on failure

conditions of sheets fabricated with hydrided zirconium alloys (illustrated in Fig. 3 for recrystallized Zircaloy 2). In Fig. 3, ϵ_1 corresponds to the axial strain in claddings and ϵ_2 is similar to the hoop strain. These room temperature test results show a large decrease in the ϵ_1 -value (\approx factor of three) as the loading path shifts from uniaxial tension to equal-biaxial tension. Furthermore, this decrease becomes even more pronounced for materials hydrided to high hydrogen contents and subjected to equal biaxial loading. Thus, for these particular material conditions, there is clearly a strong sensitivity of failure strain to both the multiaxiality of the stress state and the hydrogen content. Furthermore, Prat et al. [17] confirmed the large decrease in fracture strains between uniaxial and plane-strain tension with room temperature results showing Zircaloy-4 being brittle at 600 wt. ppm H in plane strain even though it retained significant ductility in uniaxial tension.

Given that RIA stress-state conditions are comprised between plane strain and equi-biaxial tension according to integral tests analysis, Fig. 3 indicates that the failure strain of cladding under RIA conditions may be significantly lower than the results obtained from uniaxial tension testing. Using the data plotted in Fig. 3, the ratio between hoop strains at failure under equi-biaxial loading and uniaxial tension testing can be expressed in the form of a functional relationship depending on the hydrogen content [27]. This relationship or “correction factor” can then be applied to data obtained from uniaxial tensile tests on axially short ring specimens to predict the expected multiaxial fracture strain value under PCMI loading conditions during a RIA. A similar correction function can be applied burst test results in order to predict the expected failure behavior during a PCMI loading phase in a RIA. Several RIA failure criteria that rely on such correction factors have been developed [8,28].

In an attempt to address this issue, correction factors have been derived from data such as Fig. 3 in order to determine the expected hoop strain ratio at fracture to transform mechanical test data, such as those obtained under uniaxial tension, into the expected failure strain values under equi-biaxial loading that is expected to better simulate RIA loading during the PCMI phase. Several failure criteria have been developed that rely on such correction factors [8,28].

Unfortunately deriving correction functions from data such as Fig. 3 has several limitations for applications to high fuel burnup cladding, especially under RIA conditions at elevated temperatures [29]. Importantly, Fig. 3 is based on room temperature behavior of

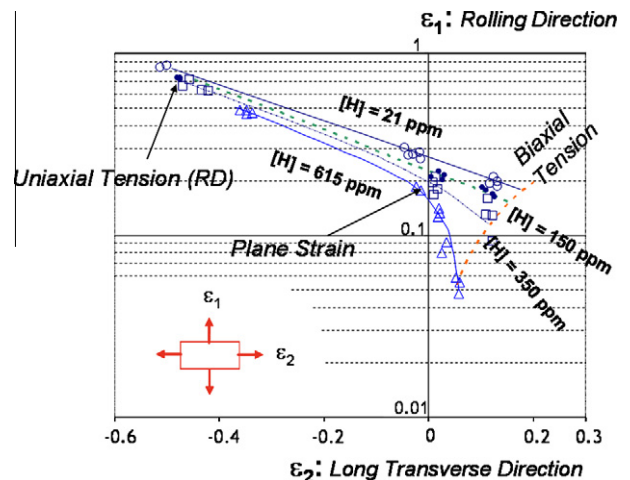


Fig. 3. A room temperature fracture limit diagram for recrystallized Zircaloy-2 sheet at four levels of hydrogen content. The values of ϵ_1 and ϵ_2 refer to the major and minor principal strains respectively in the plane of the sheet at fracture. After Yunchang and Koss [16].

unirradiated flat sheets of recrystallized Zircaloy 2 in which a significant density of hydrides was present along the grain boundaries at the high hydrogen contents. Moreover for the higher H contents, a significant amount of radial hydrides were also present [30]. Neither these testing conditions nor the material microstructures are prototypical of PWR conditions. For example, the fracture behavior in Fig. 3 at high hydrogen contents is a result of a damage accumulation process in which grain-boundary hydrides initiate voids that link along an efficient near-intergranular multidirectional fracture path under equal-biaxial tension (i.e., the local fracture path is such as is seen in Fig. 4b but on a grain-scale level). The resulting fractography shows a stress-state induced change of fracture surface appearance with significant intergranular fracture occurring under equal-biaxial tension at the high hydrogen content, resulting in very low ductility for this stress state [30]. In contrast, the commonly observed alignment of hydrides in cold worked and stress relieved (CWSR) Zircaloy cladding in the circumferential-axial direction inhibits void linking and prevents this stress-state-induced fracture path transition. Thus, much higher fracture strains are to be expected for CWSR material containing this hydride morphology subjected to equal-biaxial tension. Furthermore, at elevated temperatures (≥ 300 °C), the void initiation strain increases significantly [31–35] and consequently the hydride precipitates have a lowered contribution to the failure process; the result is higher fracture strains and (probably) a diminished role of stress state on fracture, although such data do not exist. It is thus recommended not to use the Yunchang and Koss data points to establish correction functions for elevated temperature PWR conditions for CWSR cladding. In general, great care should be taken in applying correction factors from one test to another.

3.2. Failure in the presence of a crack

The data in Fig. 3 indicate a strong sensitivity of fracture on stress state under conditions in which hydride particles cause fracture through a damage accumulation process, accelerated by a combination of stress state and the presence of grain-boundary hydrides. However, high fuel burnup cladding is often characterized by the presence of hydride blisters or rims located on the outer surface of the cladding tubes which in turn will contain a range of hydride microstructures beneath the blister. Being brittle even at elevated temperatures (400 °C), the solid hydride blister or rim forms a surface crack at a strain roughly equal to the cladding yield strain [31]. In this case, cladding failure is due to crack growth.

Prediction of failure for the case when crack growth dominates should depend on the appropriate fracture mechanics, the depth of the blister/crack, and the fracture toughness of the underlying substrate material beneath the blister. Pierron et al. [31] examined the fracture behavior of unirradiated CWSR Zircaloy-4 sheet (which has Kearns factors similar to those of fuel cladding) containing solid hydride blisters of varying depths and subjected to plane-strain deformation. The experiments relied on a lenticular hydride blister located in the center of double edge-notched flat-sheet tensile specimens that introduce a biaxial stress state in the specimen center such that plane-strain deformation is induced. That study found that at room temperature the fracture strain of the material beneath the cracked blister depended strongly on hydride blister (crack) depth. Fracture occurred in a manner that could be well predicted by crack growth dictated by an elastic–plastic fracture mechanics analysis [31]. At 300 °C, a slower decrease of fracture strain with crack depth was observed, and it could no longer be predicted using fracture mechanics, suggesting that a competing failure mechanism (with diminished sensitivity to crack depth) controls fracture.

To address the influence of stress state on failure of hydrided Zircaloy in the presence of a crack, Glendening et al. examined the contrast in behavior of the same unirradiated CWSR Zircaloy-4 sheet material, containing a solid hydride blister and fractured under either equal-biaxial tension or plane-strain tension and at temperatures of 25 °C, 300 °C, and 375 °C [18]. As shown in Fig. 4, the equal-biaxial test procedure relied on in-plane punch-stretch tests in which the sheet specimens are deformed under an equal-biaxial tension strain path, as evidenced by the “mud-cake” fracture pattern of the hydride blister in Fig. 4.

As shown in Fig. 5, the results from tests performed under the equal-biaxial conditions shown above show very similar fracture strain dependence on crack depth to those performed using the double edge-notched plane-strain ring geometry. Both test conditions show a decrease in failure strain with increasing blister/crack depth at all temperatures, and importantly, at a given blister depth and temperature, the plane-strain fracture strain values lie within experimental scatter of those determined under equal-biaxial tension. It should be noted that while Fig. 5 is based on “far-field fracture strain values” determined over the length of the 3 mm diameter blister, similar behavior is observed for local fracture strains at 0.4–0.5 mm from the fracture surface.

The results in Fig. 5 confirm that the influence of stress multiaxiality is much more limited than expected from Fig. 3. In fact, there

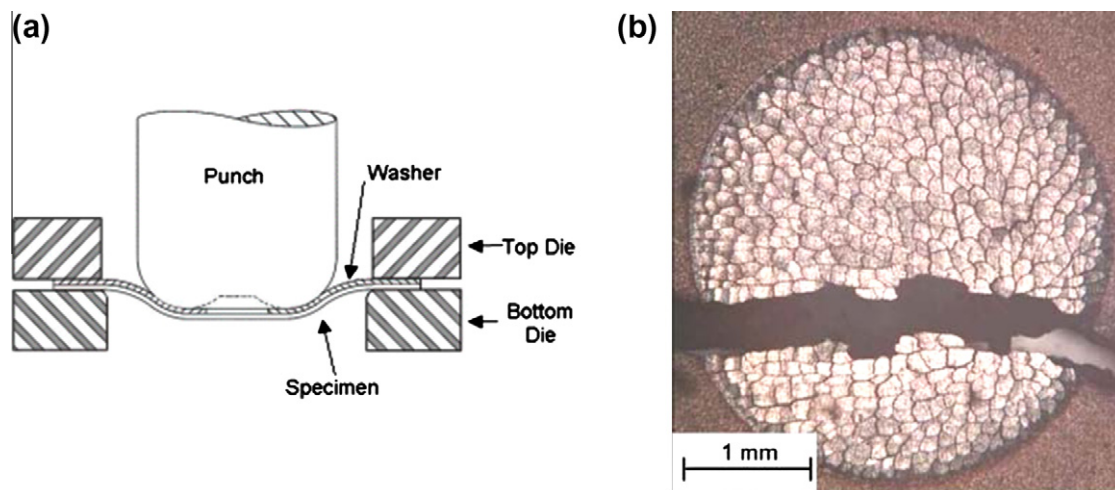


Fig. 4. (a) A schematic of equal-biaxial punch-stretch test procedure of a Zircaloy-4 sheet with hydride blister and (b) the resulting “mud-cake” crack patterns within the blister [18].

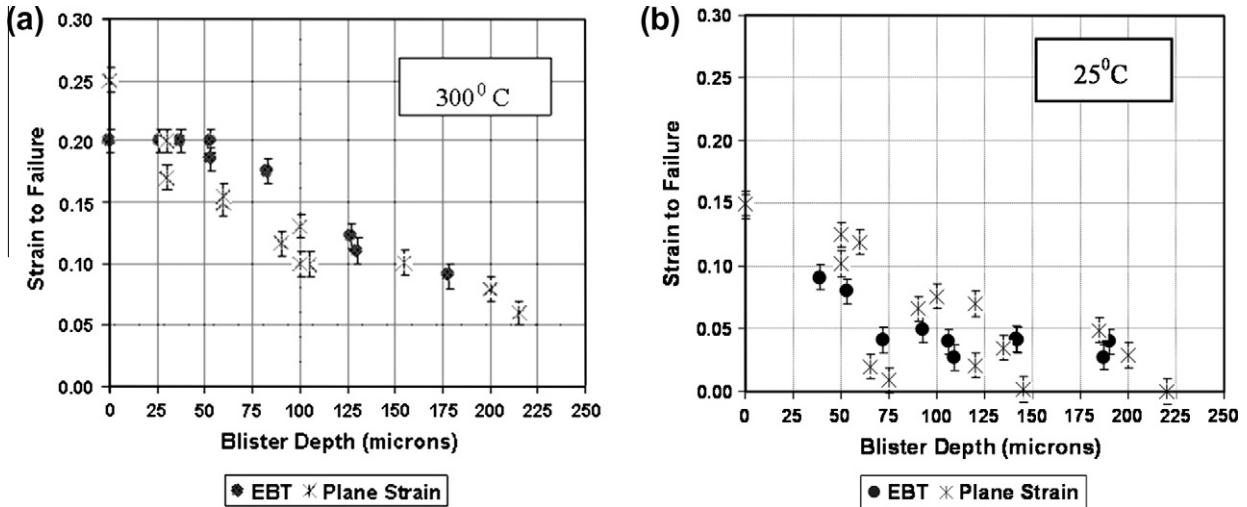


Fig. 5. A comparison of maximum far-field principal strains at failure under equal biaxial and plane strain loading for CWSR Zircaloy-4 sheet specimens containing hydride blisters of a range of depths [31,32].

is no significant effect of stress state (between plane-strain tension and equal-biaxial tension) on the fracture strains of the Zircaloy-4 under conditions where a crack dictates fracture. Rather, these data strongly suggest that, in the presence of a crack, it is the maximum principal strain value (i.e., the strain component normal to the crack surface measured far from the crack) that controls the fracture process regardless of stress state within the regime plane-strain to equal-biaxial tension. However, initial attempts to analyze the elevated temperature data using elastic–plastic fracture mechanics were not successful, probably due to extensive crack-tip blunting [33].

3.3. Summary of failure mechanisms

The determination of the appropriate failure mechanism is essential for developing a sound failure criterion. The studies show that the effect of stress state, if any, depends on the mode and mechanism of fracture, at least in the range of plane-strain

to equal-biaxial tension. Three possibilities of cladding failure mechanisms are likely:

1. If a “long”(deep) crack is present such that crack growth dictates fracture, the failure strain should be defined on the basis of maximum principal strain (or possibly stress) normal to a crack and described by the appropriate fracture mechanics formulation. Based on this criterion (i.e., ϵ_1 or σ_1), cladding failure in the presence of a surface crack should be either independent of strain path (if a critical value of ϵ_1 dictates, as in elastic–plastic crack growth or weakly dependent on σ_1 if critical value of σ_1 dictates like for near-elastic crack growth).
2. If crack initiation does not occur (or if only a very short crack is present), then cladding failure is likely to depend on a ductile fracture process that is sensitive to the details of a damage accumulation process. In that case, it has been established that void nucleation at least at low temperatures (at fractured hydrides), void growth, and void coalescence all are sensitive to stress

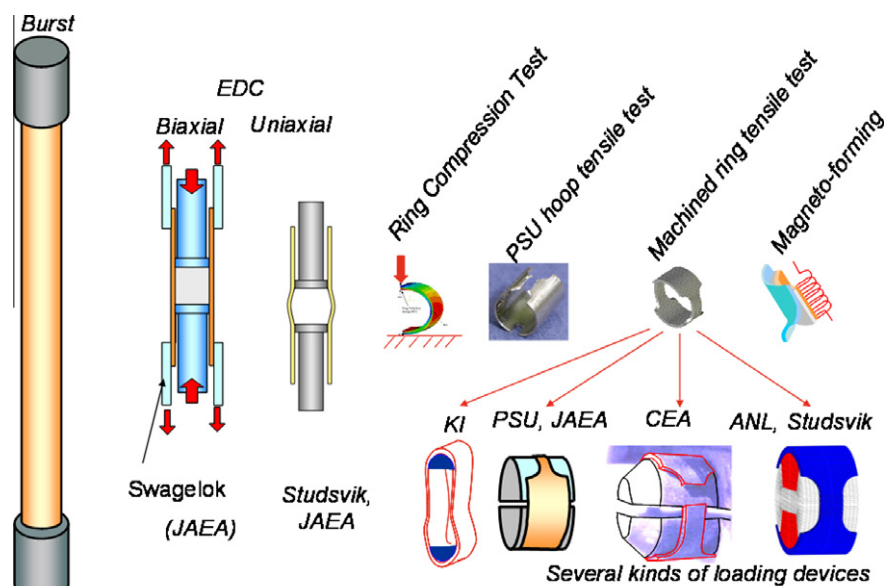


Fig. 6. A schematic depicting hoop tensile testing techniques recently used to assess the mechanical response of high burnup cladding.

state with increased biaxiality accelerating the process and resulting in decreased fracture strains. Thus, in this case, the failure criterion is dependent on stress state. Given temperature sensitivity of hydride precipitate particles to fracture [31–35], the stress-state dependence of hydrided cladding is likely to depend on temperature.

- Finally, a third option for material failure exists if crack initiation and damage initiation are both difficult, such as at elevated temperatures in hydrided Zircaloy [33]. In this case, some form of a deformation instability process (or some other ductile failure mechanism) is possible in which case sensitivity to stress state is again likely, especially if that process depends on a local plane-strain condition as in the localized necking of sheet material [34].

In view of the above discussion, the cladding failure mechanism must be reproduced in order for the mechanical testing results and modeling predictions to be accurate.

A basic consideration is the appropriate failure criterion. For failure due to an exhaustion of ductility such as due to damage accumulation, a fracture strain sensitive to strain path would be expected. In the presence of a long crack, failure associated with (through-thickness) crack growth clearly should depend on the appropriate fracture mechanics in which the crack length and the fracture toughness are central considerations. In this case, the expected sensitivity of failure to stress state should be much less than in exhaustion of ductility controlled failure. It should be noted that both damage accumulation analyses and elastic–plastic fracture mechanics analyses are sensitive to the deformation behavior of the material. Finally, alternate forms of failure such as plastic instabilities are also very sensitive to both strain hardening and strain-rate hardening (as well as stress state). In view of the above, the following discussion addresses the “usefulness” of the Fig. 6 test data to predicting RIA performance.

4. The mechanical testing of high burnup fuel cladding

This section reviews the mechanical testing configurations available for testing irradiated tubing and assesses their adequacy in reproducing the conditions experienced by cladding during a RIA.

4.1. An overview of existing hoop tensile test techniques

While the studies described in the previous section span the expected strain paths encountered by high burnup fuel cladding during a RIA, most of the test procedures used rely on unirradiated flat sheet material tested in a manner that is not directly applicable for testing high burnup cladding. Fundamental to the existing test techniques is that cladding failure occurs by fracture due to hoop expansion. As depicted in Fig. 6, the test procedures use a range of specimen geometries and several loading configurations. As a result, many techniques have evolved to determine the mechanical properties of cladding samples tested in the hoop direction. It should be noted that with the exception of the burst test procedure (which is force-controlled), the tests shown in Fig. 6 are displacement-controlled.

A central issue to this discussion is the relevance of the resulting mechanical test data from the techniques in Fig. 6 to RIA performance. As a basis for discussion, we believe that in order to predict appropriate failure conditions it is critical to predict both the deformation and fracture behavior under RIA conditions. Thus, in addition to fracture criterion data, the yield and flow behavior of the cladding as a function of strain, strain rate, and stress state (in particular to assess plastic anisotropy) form the bases for an

accurate predictions of the deformation behavior under multiaxial strain paths such as in the RIA.

4.2. Finite element modeling

Most of the described tests have been simulated using finite element modeling. The Cast3 m Finite Element Analysis (FEA) code developed by CEA [36]. Isotropic elastic–plastic behavior is assumed for the cladding. The uniaxial stress–plastic strain curve used in all the Cast3 m models is a power-law adjusted to describe the behavior of high burnup Zircaloy-4 cladding at 350 °C at 1/s strain rate. These modeling conditions are conditions of interest for PCMI loading under RIA transients.

$$\sigma(\text{MPa}) = 781 \cdot (\epsilon^p)^{0.015}$$

The Young modulus is 79,360 MPa and the Poisson ratio 0.325.

Large displacements and large strains have been systematically assumed. For simulation with contact, Coulomb frictional contact was modeled. The Cast3 m modeling imposes to use locally linear interpolation elements at the vicinity of contact surfaces. The magneto-forming test was not modeled in the scope of the present study but based on EDF calculations.

Several 2D and 3D FEA models were developed to simulate most of the further discussed tests: ring tensile tests loaded with double-D, ring tensile test with inserted dog-bone, plane strain ring tensile test, EDC test and Ring compression tests.

4.3. The burst test

The burst test is a pressure-controlled loading test which imposes a biaxial stress state such that $\sigma_{zz} \sim \frac{1}{2} \sigma_{\theta\theta}$, which should result in a near plane-strain strain path. Burst tests are usually performed with on-line measurement of strains (and strain paths) using strain gages. Usually the burst tests are pressure ramps with constant increase of pressure rates. Another pressurization test is sometimes performed by modifying the pressure rate and reaching constant deformation rate. In both cases, for sufficiently slow deformation, the strains are uniform up to the uniform elongation strain (UE). Thus the boundary conditions are accurately known during a burst test, and this test provides a very precise determination of the cladding mechanical yield and deformation properties at small strains. The resulting stress–strain response can only be described up to hoop strains roughly equal (assuming isotropic plasticity) to the uniform elongation ($\sqrt{3} \cdot \text{UE}/2$), where UE is the Uniform Elongation obtained in a uniaxial tension test. For strains greater than $\sqrt{3} \cdot \text{UE}/2$, the cladding tube is susceptible to a plastic instability commonly known as localized necking, which is common in ductile sheet metal forming. Under a plane-strain deformation path (such as is the case for the internally pressurized closed end cladding tube), the onset of localized necking occurs at a maximum principal strain roughly equal to the strain-hardening exponent n for a thin-wall tube of nearly uniform thickness. For a uniaxial tensile test, $\text{UE} \approx n$ (the strain-hardening exponent), and thus a thin-wall cladding tube should fail during a burst test at hoop strains roughly equal to the UE-value from a tensile test. However, deviations from this behavior can occur in the presence of any thickness imperfection, such as a cracked hydride rim, which will decrease the failure strain due to crack growth or accelerated localized necking.

It is possible to estimate a value of the *total elongation* (TE) of a fractured burst test specimen [37–39]. For example, it is possible to determine the final cracked tube perimeter either by wrapping the failed sample with an aluminum sheet [37] or from several diameter measurements at a given axial location. In both cases, the crack opening displacements must be subtracted to determine a

“total elongation” value for the hoop strain. When several axial locations are analyzed, the total elongation values tend to show considerable scatter in magnitude, and thus these values derived from burst tests are not always very accurate. Another concern when deriving TE value is that the strain rate for the deformation occurring between UE and TE can be very high on a local basis, and it is not controlled. In addition, the local stress/strain states are not controlled after UE and will also vary spatially.

Of the tests depicted in Fig. 6, the burst test is likely the most sensitive to the condition of the cladding surface and to the presence of defects. This situation arises from a combination of the large specimen surface area and the fact that the load transferred along the perimeter of the cladding tube increases the stress at any imperfection. Thus, the stress will concentrate in any section that has a reduced load-carrying capacity, especially in the presence of a linear imperfection or crack aligned along the axis of the cladding tube, such as in the case of a surface crack. As a result, the burst test can be very useful in determining the presence of embrittlement along the cladding surface. For the case of cladding with hydride rims of limited ductility, the cladding will tend to fail at a location corresponding to the deepest hydride damage. For example, Fig. 7 showing a complex crack path in which the failure mode is controlled by a series of simple process illustrated in Fig. 8, but it is initiated within a central section where the incipient crack depth is greatest. Consequently, burst tests provide data on the maximum depth of hydride damage if such damage is sufficiently deep to influence the process [37].

In the early eighties, burst test technique at both low and high temperature was still introduced into hot cells [39]. For testing temperatures below 500 °C, oil pressurization is preferred and at higher temperature, gas pressurization using helium is usually preferred. The change of pressurization media is linked to the potential dangers associated to oil burning.

4.4. Ring tensile testing

As depicted in Fig. 6, there have been several different specimen/grip configurations used to characterize the deformation behavior of high burnup cladding under a hoop tensile mode. In all cases, the tests impose a displacement to the test specimen. Importantly, in all cases the configuration of both the grips and the test specimen either impose bending or introduce a friction component to the deforming section of specimen. As a result, experimental procedures can be employed to determine the resulting local strains, strain distributions, and UE values as well as total elongations TE. However, a determination of the accompanying stresses usually requires computational analysis and an assumption of the friction between the specimen and grip/mandrels. The following section briefly reviews some of the current test procedures for determining the deformation and fracture behavior of high burnup cladding subject to hoop expansion.

Ring or hoop tensile tests typically rely on D-shaped grips or mandrels that stretch the ring shaped specimen. If the mandrel diameter is significantly smaller than that of the cladding tube, as in the Kurchatov Institute test (“KI” configuration in Fig. 6, described with details in [40]), then extension of the ring causes a

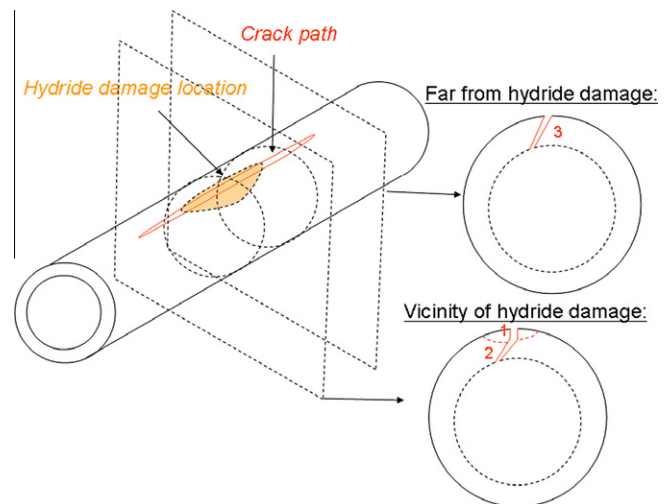


Fig. 8. Schematic description of the three step failure process when burst testing hydrided cladding (1: incipient crack nucleated in the axial-radial direction located in the deepest hydride damage, 2: crack propagation towards the inner diameter, 3: axial propagation).

bending phase that stops when the inner diameters becomes adjusted to the outer diameter of the mandrels. As a consequence of this bending, a non-uniform hoop stress distribution will develop within the cladding thickness with tension stress at the inner diameter and compression stress at the outer diameter. The bending might thus slightly delay the failure of an irradiated sample containing a hydride rim at the outer diameter, although the deformation/fracture behavior of (straightened) cladding wall can be determined.

The above problem can be minimized by the use of double-D mandrels with diameters adjusted to the sample inner diameter; see Fig. 6. However, aligning the gauge section with the opening between the mandrels still induces a bending strain to the specimen gauge section as the mandrels separate during the test. However the use of double-D mandrels must also be considered carefully due to the adverse influence of local shear at the end of contact between mandrel and sample that can promote failure from the inner side of the sample. This effect is well known for blade-disk contact in aircraft engines industry and is responsible of numerous blade failures and sometimes of crack nucleation in rotating disks [41,42].

A more efficient way to reduce the bending consists of inserting a so-called “dog-bone” between mandrels [43]. In this configuration (see Fig. 6), deformation of the ring specimen helps maintain a self-similar circular cross-section as bending within the gauge section is inhibited by the dog-bone insert. However, now there is direct contact between the surfaces of the insert and specimen gauge length in a manner that introduces significant non-uniform frictional forces, increasing toward the midpoint of the gauge section.

While local strains can be measured experimentally in “dog-bone” ring tests, finite element analysis is required to establish

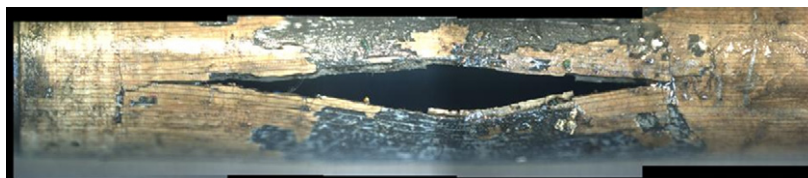


Fig. 7. Post-test aspect after burst testing at 280 °C with pressurized oil a 75 GwD/tU a zirconium alloy cladding with a 100 μm thick oxide layer.

the stresses within the specimen because of the presence of friction. For example, Arsène and Bai [43] demonstrated that the engineering hoop stress is modified by friction and geometry, such that:

$$\sigma_{\theta\theta} = \frac{F}{S_0} [1 - f_c(\Delta L; f)] \quad (2)$$

$\sigma_{\theta\theta}$, averaged hoop stress in the center of the gage section; F , applied force (to the mandrels); S_0 , initial gage area; ΔL , machine displacement; f_c , stress correction function. If $f_c = 0$, the engineering stress–strain curve can be derived directly from raw data like in a standard uniaxial test. If f_c increases less force has to be applied to achieve material yielding; f , friction coefficient between specimen and D mandrels.

The f_c -function may be calculated by finite element analysis, assuming a static friction coefficient, and some of the results are illustrated in Fig. 9 for Zircaloy-4 ring specimen loaded with a dog-bone spacer between the mandrels. A surprising conclusion is that the stress correction on hoop stress (f_c) is reduced in the central section of the gauge section by increasing the friction coefficient. The force components applied to the sample by the loading device are represented in Fig. 10. At a given applied force, increasing the friction coefficient, which causes an increase in the y -direction component F_y and thus decreases the f_c function, which is consistent with the finite element calculation results plotted in Fig. 9.

Similar conclusions of friction effects were drawn from analysis within the PROMETRA program [44] in which finite element modeling of hoop tensile tests were performed on ring samples with machined gage section loaded with double-D mandrels. Comparing the force–displacements measured during mechanical testing and calculated by finite element simulations, the friction coefficient was assessed in several testing conditions for axially short ring tensile tests of the PROMETRA program. Those results predict that in the absence of lubrication the static friction coefficient is close to 0.4 for both fresh and irradiated cladding samples. These simulations also predict that the stress–strain curve is obtained, with acceptable accuracy, dividing the applied load by gage area and applied displacement by gage length for a 0.4 friction coefficient. The stress correction function is non-negligible in the range of small displacements (see Fig. 9), in other words UE is affected by some uncertainty whereas TE is more accurately determined.

In summary, proper analyses of the ring tension tests either with double-D mandrels or the combination of double-D mandrels and dog-bone inserts can serve to provide reasonable estimates of the hoop stress–strain response for strain paths near-uniaxial tension. In the case of hoop tensile tests on axially short ring samples

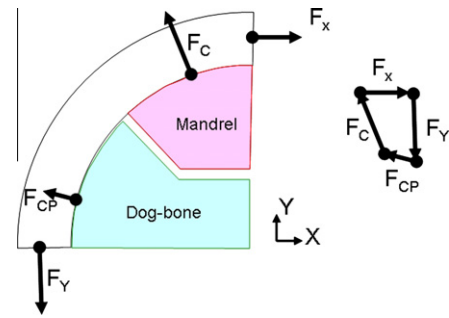


Fig. 10. Representation of the efforts applied to cladding sample during a ring tensile with inserted mandrels and dog-bone.

(gage section is 3 mm long and 2 mm wide) tested with inserted mandrels, Fig. 11 shows that the stress and strain biaxiality in the center of the gauge section at the outer diameter remain relatively constant and biased towards pure shear such that at larger strains ($\epsilon_{\theta\theta} \geq 0.06$):

$$\frac{\epsilon_{zz}}{\epsilon_{\theta\theta}} \cong -0.7 \quad \text{and} \quad \frac{\sigma_{zz}}{\sigma_{\theta\theta}} \cong -0.5 \quad (3)$$

Importantly, the above calculations indicate that strain path ($\epsilon_{zz}/\epsilon_{\theta\theta} = -0.7$) and stress state ($\sigma_{zz}/\sigma_{\theta\theta} = -0.5$) within the gauge length of the axially short ring tensile test are not at all close to the positive biaxiality experienced by cladding during the RIA event (Table 1 showed $\epsilon_{zz}/\epsilon_{\theta\theta} = 0.0\text{--}0.7$ implying that $\sigma_{zz}/\sigma_{\theta\theta} = 0.5\text{--}0.9$). While the stress states within other ring tensile test geometries will also be sensitive to specimen gauge length-to-width ratios, even those with larger ratios, such as the ASTM prescribed ratio of 4:1, still results in a near-uniaxial tension strain path ($\epsilon_{zz}/\epsilon_{\theta\theta} = -0.5$) such that ($\sigma_{zz}/\sigma_{\theta\theta} = 0$). Thus, while stress–strain behavior may be deduced from analysis of such test data, any experimental failure strain-value would require a large “stress-state correction” in order to use such data for prediction of RIA behavior. Furthermore, the accuracy of the UE-value at maximum load is probably limited because in the domain of small strains, the influence of friction is not negligible, especially for irradiated cladding material with its rough internal surface.

In order to eliminate specimen bending and to maintain the circular cross section of the specimen, the gauge sections in the JAEA hoop tensile tests are placed on the upper mandrel with a 90° rotation when compared to other ring tests; see Fig. 6. In such a configuration, the large normal stress acting on the gauge section would normally impart a large friction stress. In order to reduce friction in

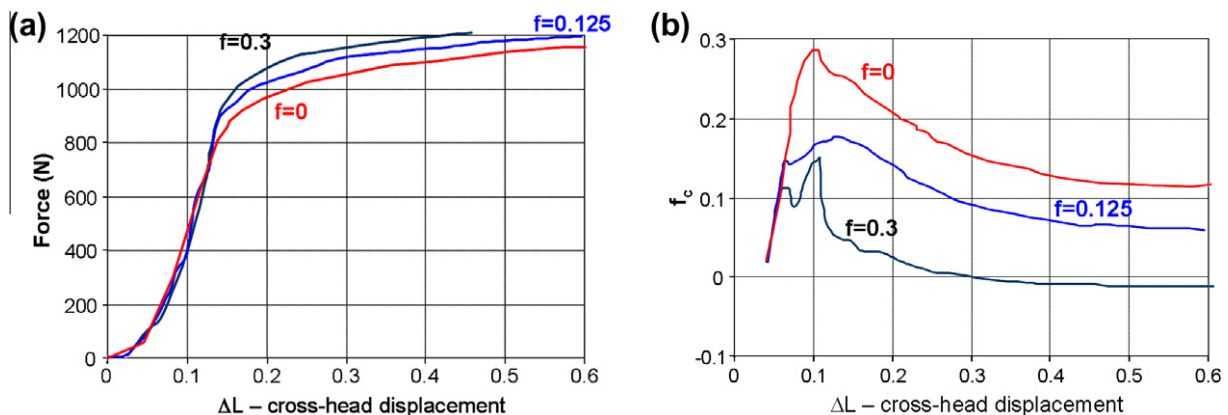


Fig. 9. Finite element calculation of a ring tensile test with inserted mandrels and dog-bone, influence of friction between loading device and tested sample [43,45–47]; see Eq. (2) for definition of f_c .

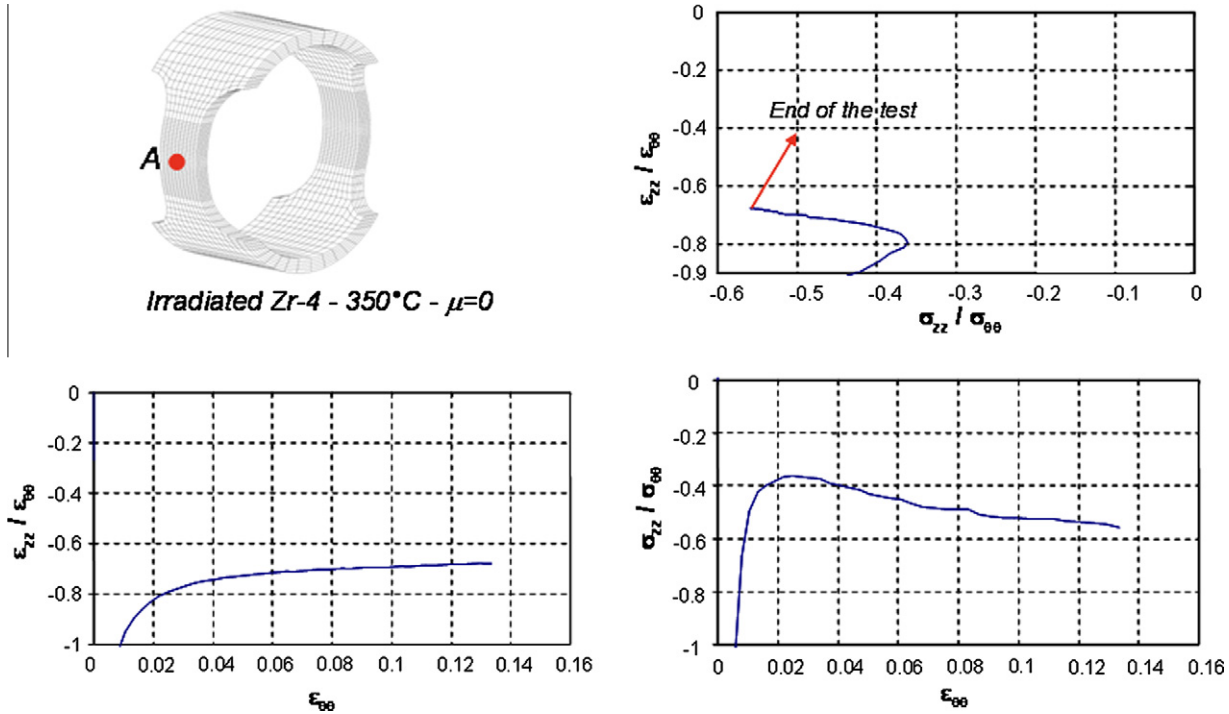


Fig. 11. Three-dimensional finite element modeling of the axially short ring tensile test with a gage section 3 mm long and 2 mm wide (zero friction coefficient is assumed between the sample and mandrel).

such a configuration, the mandrels are coated with Teflon (PTFE) tape. However, determining the resulting stress–strain response requires not only finite element analysis but an accurate knowledge of the friction coefficient; while likely small (probably in the range of 0.05 for Teflon tape), the presence of friction will nevertheless have a significant influence on the effective stress that the load imparts to the specimen in this configuration. In the JAEA hoop tensile tests, a “failure strain” can be determined experimentally, but frictional effects dictate a non-uniform strain distribution along a gage section of uniform width. The use of a PTFE tape limits the maximum testing temperature to about 330 °C.

Ring tensile tests were introduced in hot cells in the early nineties and cladding samples were tested under close to RIA conditions at high temperatures. Examples of the failure behavior of both hydride-embrittled and ductile ring sample of irradiated Zircaloy-4 appear in Fig. 12. The ductile failures always have a macroscopic fracture plane inclined at 45° to the stress axis. However, such failures are never observed during RIA testing on fueled rodlets. In this case, the frequent brittle behavior is characterized by a fracture plane whose trace is normal to the stress axis, as shown in Fig. 12.

4.5. Expansion due to compression (EDC) tests

Developed at Studsvik Nuclear and tested in hot conditions [10,48,49] and evaluated at JAEA (Japan Atomic Energy Agency) [50] and at CEA (Commissariat à l’Energie Atomique) [51], the EDC test consists in axially compressing a polymer pellet inserted into the cladding sample between two pistons. As depicted in Fig. 13, the hoop expansion of the polymer pellet induced by axial compression deforms the inner wall of the cladding. Diameter measurements are continuously recorded, the force applied to the pistons is monitored as well. An analysis of the cladding deformation as it expands during the test requires recognition of several frictional effects. Specifically, as shown in Fig. 13, there is friction at the following: (a) the piston–pellet interface, (b) the

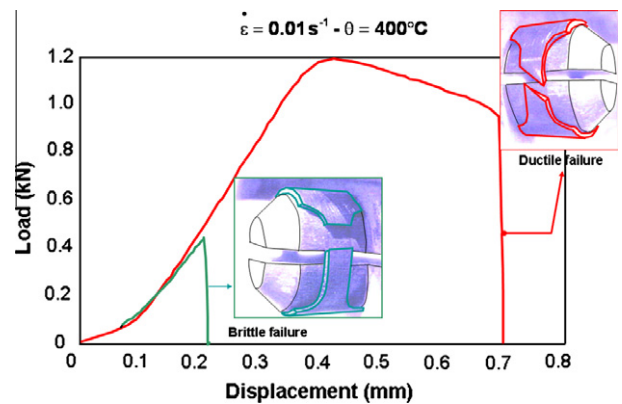


Fig. 12. Ring tensile tests performed using double mandrels – failure aspect of both ductile and brittle samples.

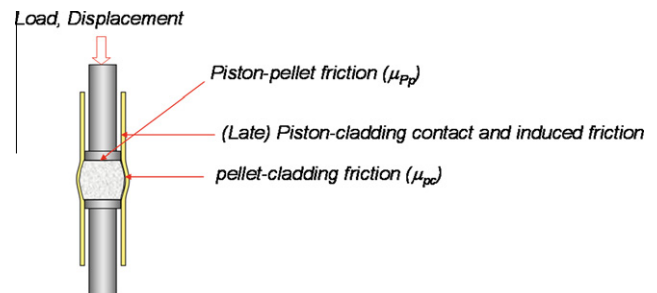


Fig. 13. The expansion-due-to-compression (EDC) test and related frictional effects.

pellet–cladding interface, and (c) for large deformations of the cladding, the interface between the cladding and piston sometimes causes a noticeable friction effect. As a result, the EDC test is not

well suited to derive accurate Yield Strength (YS) or Ultimate Tensile Strength (UTS) values.

The stress state and the strain path in the EDC test may be estimated by Finite Element Modeling (FEM) taking into account complex contact between parts [49]. Fig. 14 shows an axisymmetric finite element analysis for the evolution of the strain-path and stress-states as a function of hoop strains ($\epsilon_{\theta\theta}$) up to 0.1 for a location along the radial-circumferential symmetry line at the outer diameter of the cladding sample assuming friction coefficients of 0.2 and 0.4 for the piston-polymer interface and the pellet-cladding interfaces, respectively. Importantly, Fig. 14 shows that the strain path ($\epsilon_{zz}/\epsilon_{\theta\theta}$) is quite constant and has a value ($\epsilon_{zz}/\epsilon_{\theta\theta}$) ≈ -0.5 . Taking into account the friction effects, the corresponding stress state ($\sigma_{zz}/\sigma_{\theta\theta}$) increases somewhat with strain ranging from ($\sigma_{zz}/\sigma_{\theta\theta}$) ≈ -0.2 at ($\epsilon_{\theta\theta}$) = 0.02 to ($\sigma_{zz}/\sigma_{\theta\theta}$) $\approx +0.2$ at ($\epsilon_{\theta\theta}$) = 0.10. Decreasing the pellet-cladding friction coefficient slightly increased both the stress ratio as well as the strain ratio; however, this effect has a low influence. These stress and strain ratios are a characteristic of the EDC test and will not change significantly with material properties. The FEM also shows that, the hoop strain is quite homogeneous across the cladding thickness. It should be noted that the gage length of EDC sample corresponds to the entire perimeter of the cladding; so in that capacity, this test is representative of the RIA conditions.

The stress and strain ratios during an EDC test correspond to those close to uniaxial tension:

$$\frac{\epsilon_z}{\epsilon_\theta} \cong -0.5 \quad \text{and} \quad \frac{\sigma_z}{\sigma_\theta} \cong 0 \quad (4)$$

Because of this, while the EDC test offers a conveniently simple experimental solution to determining the failure strain of high burnup cladding in which the entire perimeter of the cladding is subjected to deformation, the failure strain values still require a significant stress-state correction to be applied to the prediction of RIA behavior. Efforts are underway on the possibility to add an axial loading component (biaxial EDC) in several laboratories. The test temperature has an important impact on the pellet material

to use (PTFE below 330 °C, aluminum and copper pellets were also evaluated at higher temperature [51]).

The macroscopic failure aspect of brittle cladding material tested with EDC technique is similar to the one observed during integral RIA tests performed fuel rodlets as illustrated in Fig. 15. Strain rates of about 1/s can be achieved using EDC test [51].

4.6. Ring compression tests

As depicted in Fig. 16, the ring compression test is based on compressing a ring of cladding tube of uniform width along a single radial axis, thus bending and collapsing the ring to “failure”. This straight-forward test can be readily performed on high burnup cladding and has several other advantages in that (a) there is no influence of friction between sample and loading device, (b) plane-strain deformation conditions should develop within an extended area (for axial ring extension over 10 mm), and (c) finite element simulation of the test is straight-forward [53]. The loading is close to pure bending conditions in which the maximum (tensile and compressive) strains occur at the outer and inner cladding surfaces, respectively. Consequently the material properties derived from such tests are obtained assuming that compressive material properties are similar to those in tension [53]. This is not the case if crack initiation occurs near the outer cladding surface, such as would occur if a hydride rim or blister were present.

Assuming no crack is present, the compression of a Zircaloy-4 ring sample between two planar plates has been modeled using the Cast3m finite element code, and the strain path as well as stress state have been calculated at the point marked ‘A’ located at the axial radial symmetry plane and in the middle of the outer diameter of the sample. As shown in Fig. 16, the strain path ($\epsilon_{zz}/\epsilon_{\theta\theta}$) is quite constant at the outer mid-surface location with a value very near to that of a plane-strain condition, as one would expect in bending a relatively wide strip. The corresponding degree of stress biaxiality ($\sigma_{zz}/\sigma_{\theta\theta}$) is significant as it increases with strain such that ($\sigma_{zz}/\sigma_{\theta\theta}$) ≈ 0.5 at ($\epsilon_{\theta\theta}$) = 0.02 to ($\sigma_{zz}/\sigma_{\theta\theta}$) ≈ 0.7 at ($\epsilon_{\theta\theta}$) = 0.25. Importantly, for high burnup cladding that typically

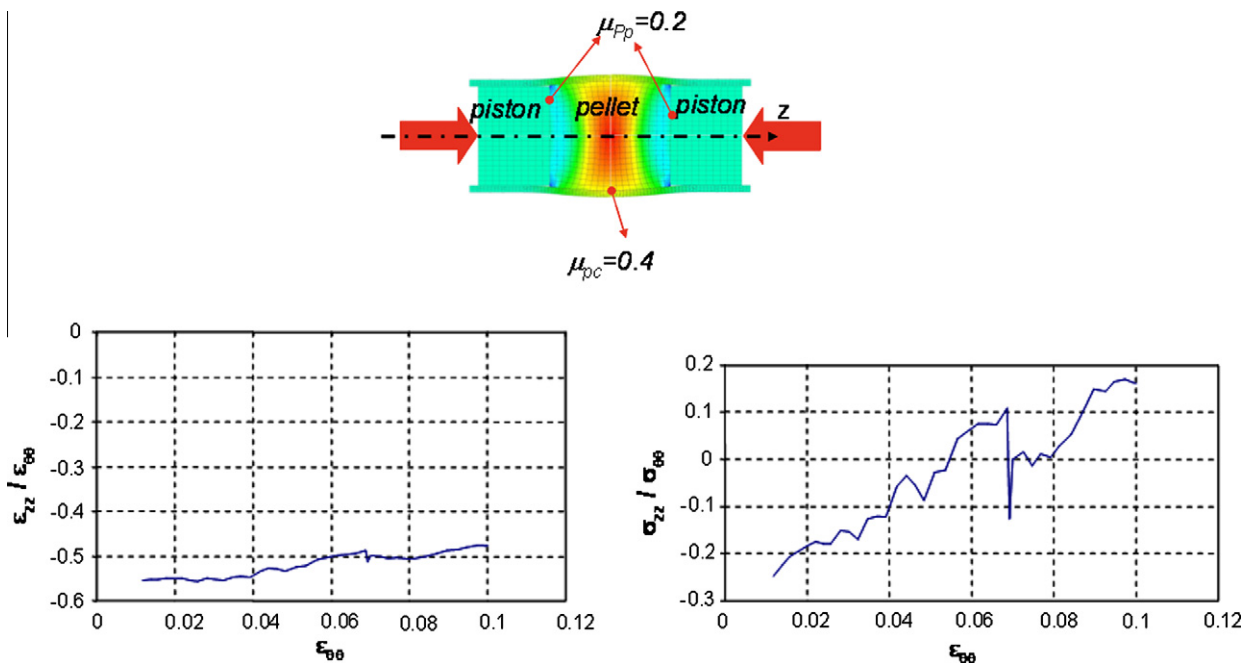


Fig. 14. A finite element model of the EDC test and the resultant predicted behavior of the strain path (at the outer diameter and most deformed location) and stress biaxiality as a function of hoop strain.

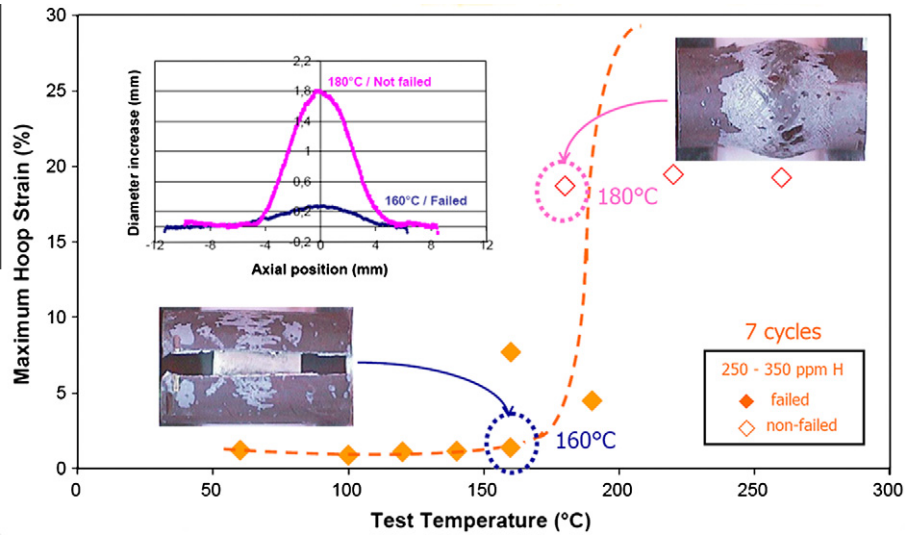


Fig. 15. Failure aspect of EDC tests performed on high burnup BWR claddings, brittle failure aspect at low temperature and deformed ductile EDC sample at higher temperature ([52]).

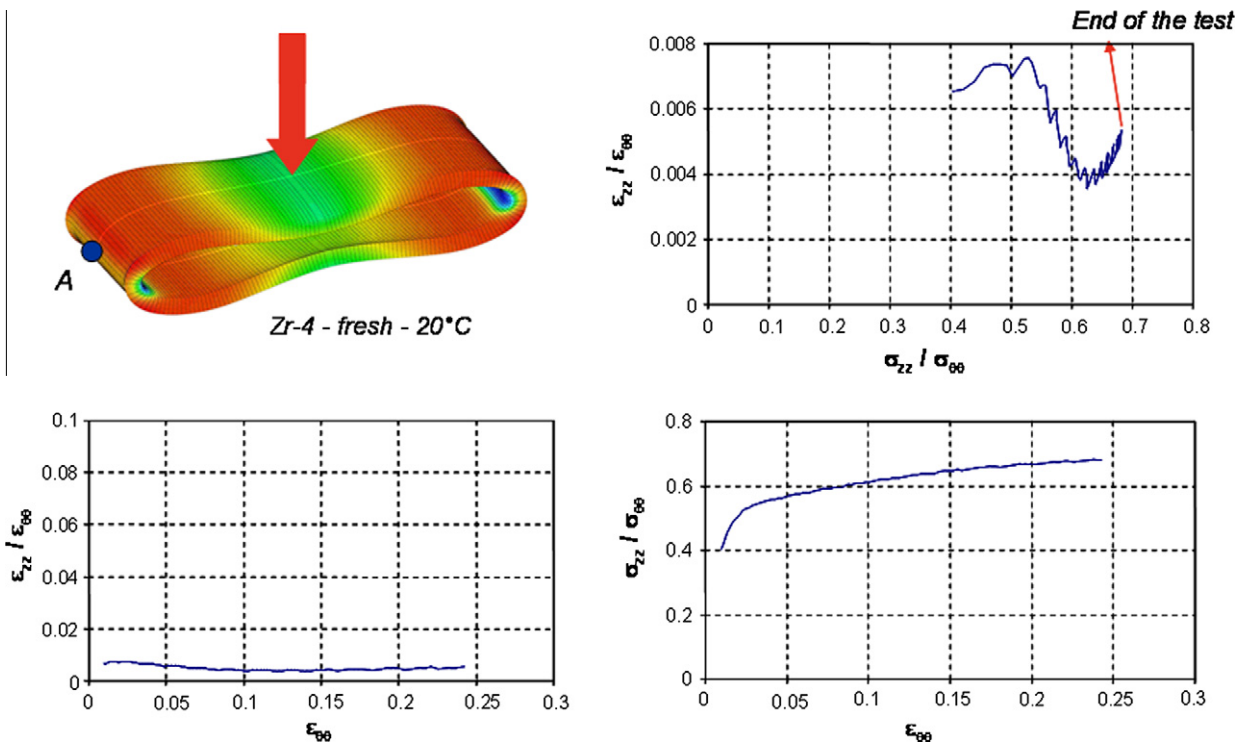


Fig. 16. A finite element model of a ring compression test of a 10 mm long Zircaloy-4 ring sample and the predicted strain path and stress biaxiality as a function of the hoop strain.

will fail at $(\epsilon_{\theta\theta}) \leq 0.10$, the strain-path and stress-state strain ratios are relatively constant at this location such that:

$$\frac{\epsilon_z}{\epsilon_\theta} \cong 0 \quad \text{and} \quad \frac{\sigma_z}{\sigma_\theta} \cong 0.5 \quad (5)$$

Thus, the ring compression test provides a significant level of stress biaxiality, making it more consistent with RIA conditions than the previously discussed ring tension and EDC procedures.

While the degree of stress biaxiality makes the ring compression test attractive for cladding assessment for RIA purposes, the nature of the test itself makes it difficult to translate test results

to either stress–strain behavior or to a failure criterion that can be utilized in a predictive model. For example, the strong strain gradient through the thin cladding wall thickness makes this test very sensitive to the surface condition in the thin strip of material that locally is subjected to large tensile strain. The small width of this strip also raises the issue of specimen scale effects. Unlike the tube burst test that subjects the entire cladding tube surface to high stresses, the ring compression test confines deformation to a small fraction of the total surface area. Furthermore, sample failure usually corresponds to the initiation of an incipient surface crack close to point A location, but experimental determination of

the local failure initiation strain is difficult, and finite element modeling must be relied onto estimate the local failure condition. Also, in cases when the inner wall of the cladding is embrittled, failure first takes place at the inner wall at a location beneath the loading contact area, again making an experimental determination of the failure condition difficult. In summary, due to its ease of performance, the ring compression is an attractive screening test to compare the *relative* failure performance of different claddings, but its nature makes it difficult to extract failure strain values that can be used as a general failure criterion for RIA response.

4.7. Plane-strain tensile test procedure

The plane-strain specimen (PSU specimen) geometry was designed at Pennsylvania State University by Link et al. [54] based on earlier research by Kampe and Koss [55] and Wagoner [56] which showed that a near plane-strain strain path could be introduced within the central region of a double edge-notched tensile sheet specimen. This technique was adapted to the Zircaloy cladding tube geometry using a ring sample with reduced gage section developed by Link et al. [54], as illustrated in Fig. 17. The sample is loaded with double-D mandrels with gage sections located in the middle of the mandrels with the mandrel-specimen interface lubricated by Teflon tape to minimize friction effects. Local strain measurements are derived from low load Vickers hardness indentations within the gage section. Both experimental measurements and finite element analysis indicate that the resulting deformation path is near plane-strain extension over the central 1/3 of the gage width. Importantly, this region is the location of failure initiation within a ductile specimen, and thus, failure in such a case occurs under a stress state close to plane-strain conditions. In material with limited ductility, the strain concentration at the notches may initiate fracture at these locations under a local stress state near-uniaxial tension. Depending on how the specimen is gripped, there may be no bending in the test procedure (the cross section diameter remains self-similar) in which case the deformation through the cladding wall thickness is uniform (as in [54]).

This test procedure was adapted at CEA Saclay within the PROMETRA program to be tested in hot cells. CEA recently developed a speckle painting technique [57] to derive local strains from image analysis (see Fig. 17), which in the original testing was performed using hardness indents. The plane-strain specimen loading was modified by CEA by positioning the gage section between the mandrels in order to limit friction effects in the absence of a lubricant between the specimen and mandrels. Those results also confirmed a plane-strain loading condition. Thus for this specimen geometry, the stress and strain ratio can be considered to be close to: $\frac{\epsilon_z}{\epsilon_\theta} = 0$ and $\frac{\sigma_z}{\sigma_\theta} = 0.5$.

The specimen geometry and the test procedure (in which significant interface friction may be present between the specimen and mandrel) imply that the material stress–strain parameters cannot be accurately determined without a complex finite element calculation. Also, since there is no well-defined gage length, the failure strains must be measured *locally* in the vicinity of the fracture. That procedure yields two indications of the failure strain: the far-field strain and the peak fracture strain, as determined at the fracture surface. The far-field strain just before specimen fracture is the strain value that can be compared to strain values obtained with RIA simulation codes that do not include the presence of an incipient crack, and this value may be considered with reference to a failure criterion for RIA.

The strain rates achieved during the PSU tests are the same than for conventional ring tensile tests. However, when using digital image correlation to determine strain maps, it is necessary to limit the strain rates in order to acquire a sufficient set of images and more specifically some images close to the failure strain. In recent years, the technique has been used in hot cells [57] and has shown that tests performed using irradiated material often fail in a complex manner leads when the plane-strain ring tensile test is used. Specimens with deep hydride rims at the outer diameter of the cladding form incipient cracks close to the notches and thus in a region that is not under the plane-strain condition. If the cladding material has intermediate ductility, through-thickness shear deformation can concentrate at the inner diameter of the cladding at the

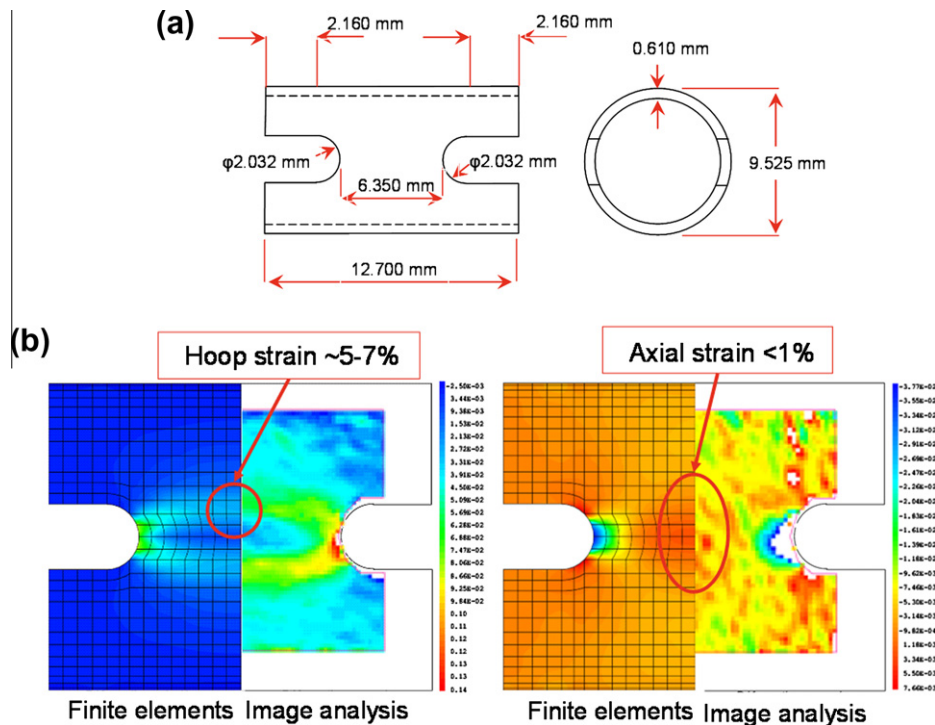


Fig. 17. (a) The plane-strain ring specimen ([54]) and (b) a speckle painting image analysis for strain measurements (other examples in [57]).

location of the edge of the mandrels, leading to incipient crack nucleation at this location. This failure mode was evidenced on metallographs and also confirmed by 2D finite element calculations. For large displacement at failure, ductile fracture is expected in the center of the plane-strain region. The PSU test still requires some developments and testing to achieve a full understanding of the generated results.

4.8. The magneto-forming test

Under development at EDF (Electricité de France), the magneto-forming test is a high strain-rate forming procedure based on a current pulse through a copper solenoid that in turn causes an expansion of the surrounding cylindrical copper driver. As illustrated in Fig. 18a, the driver expands the cladding tube which in turn is constrained to deform by an external shell with an elliptical opening. The test thus is essentially a constrained elliptical bulge test in which the choice of the geometry of the elliptical opening controls the strain ratio at the peak (i.e., outer surface) of the bulge, as illustrated in Fig. 18b [58]. If specimen failure can be avoided at the plane-strain condition imposed at the perimeter of the bulge, the peak of the bulge should deform in a biaxial strain path given by the relationship in Fig. 18b. The test is rapid, occurring on a scale of several μ s, so that the strain rate is quite high.

While the magneto-forming test can impose an eventual multi-axial strain-path of the outer surface element close to the one obtained during a RIA, Fig. 19 shows that the biaxiality of the deformation path is predicted to increase with strain from roughly a plane-strain path near yielding to a near equal-biaxial tension path at the limit of dome height [59]. Thus, failure occurs in the presence of a significant change in deformation path during the test. In addition, the geometric constraint of the “matrix” results in a combined (stretch + bending) mode of deformation to

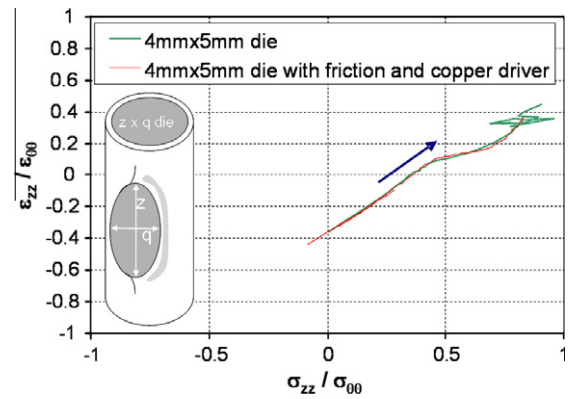


Fig. 19. Finite element simulation of magneto-forming testing stress–strain path [58]. Arrow indicates time during the test.

the specimen. Given the initial 2 mm radii used for the curvature of the matrix hollow, there is a large deformation gradient through the cladding wall (of the order of 0.13 for a 0.6 mm thick cladding) such that the inner wall may still be in compression at fracture initiation on the outer surface of the cladding. As in the PSU plane-strain tests, failure strain-values depend on measurements of local strains derived from grid marking in early tests [59]. While the test is not well suited to determine the stress–strain response of the cladding tube, the magneto-forming test is attractive in that, at least at the outer surface element, it imposes the stress and strain ratio in the range of $0.0 \leq \epsilon_{zz}/\epsilon_{00} \leq 0.5$ and $0.5 \leq \sigma_{zz}/\sigma_{00} \leq 0.8$. It is unlikely that the magneto-forming test could be introduced into hot cells. However, the influence of stress biaxiality can be studied using fresh material.

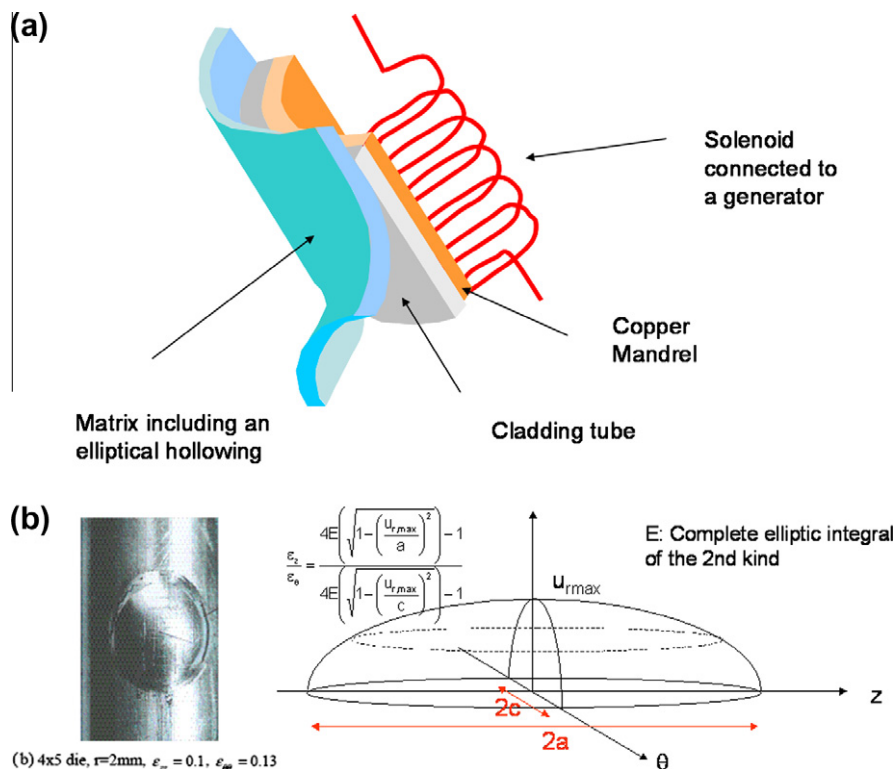


Fig. 18. (a) A schematic of the magneto-forming test of a cladding sample and (b) the resulting specimen deformation and predicted strain path as a function of specimen geometry [58].

5. Comparison of hoop tensile tests with RIA loading conditions

As a summary, the stress states and strains paths imposed by the various hoop tensile tests procedures are compared in Fig. 20 with those of the loading conditions observed after RIA integral tests in the CABRI reactor. This comparison shows that in terms of strain path and stress biaxiality, the short ring tests as well as EDC tests are characterized by stress states that are quite different from those experienced by cladding during the RIA. Thus, while these tests may be used to obtain relevant constitutive plastic flow properties of the cladding, any failure data may be subject to a large correction for the difference in stress states. For example, the short gage length ring specimen can be used to determine

the yield stress and the stress–strain response as well as the uniform elongation-value can be assessed using axially short ring, but the value is expected to be identified with a limited accuracy.

Fig. 20 shows that several tests come close to simulating the RIA loading conditions. While none of the tests exactly duplicate the RIA stress state, the burst test, the ring compression tests, the PSU plane-strain tests, and the magneto-forming test all subject the material to strain paths of interest. These tests can provide mechanical test data requiring comparatively small “corrections” to account for the differences in stress state from that of the RIA. However, as summarized below, each of these test procedures have limitations in duplicating the precise failure conditions associated with the RIA. Table 3 summarizes the comparison of the various

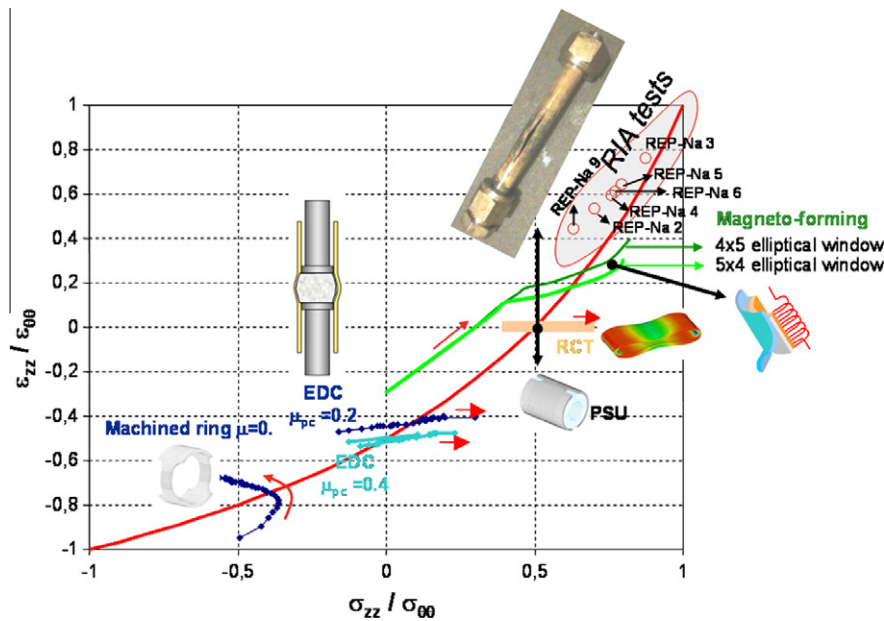


Fig. 20. A comparison of the strain paths and stress states of the various hoop tensile tests with respect to RIA loading biaxiality.

Table 3

A comparison of various test procedures used to evaluate the mechanical performance of cladding for RIA conditions.

Issues	Test					
	Burst test	Ring tensile	Expansion due to compression	Ring compression	Plane-strain tension	Magneto-forming
Compare to RIA strain path?	Good	Poor	Poor	Good	Good	Very good
$\epsilon_z/\epsilon_\theta$ [$(\epsilon_z/\epsilon_\theta)_{RIA} \approx 0.2-0.6$]	=0	≈ -0.7	$= -0.5$	=0	=0	≥ 0
Bending-induced strain gradient	No	Very small	No	Yes	No	Yes
Stress–strain response?	Yes, good to small ϵ	Yes, good if FE assisted	Yes, but only if FE assisted and friction is known	No	No	No
UE failure strain?	Fair, may be limited by “flaws”	Good	Good	NA	Good	NA
Failure strain? $\epsilon_{fracture}$	Poor	Good	Good	Fair	Good	Good
Failure strain? $\epsilon_{crack\ growth}$	NA, but sensitive to cracks	NA	NA	NA	NA	NA
Requires FE analysis?	No	Yes for $\sigma-\epsilon$ analysis	Yes	No	No	No
Is friction an issue?	No	Yes	Yes	No	Yes	Yes
Analysis: gage Area (mm ²)	≈ 3000	10	≈ 300	Few	≈ 4	NA
Material consumption (mm tube)	≈ 100	2.5	\approx few mm’s	10	12	Several mm’s
Major limitation	$\epsilon \leq UE$	Stress biaxiality	Stress biaxiality	Strain gradient + FE required	Strain measurement	Strain measurement + strain path changes

hoop tensile tests with regard to the determination of several mechanical parameters specifically for RIA performance of cladding. In terms of the relevant strain path/stress state, four test procedures (burst tests, ring compression tests, plane-strain tension and magneto forming) are relatively close to the multiaxial conditions [$(\varepsilon_{zz}/\varepsilon_{\theta\theta}) \approx 0.2\text{--}0.7$] experienced by cladding during a RIA event. Of these, the burst test can provide yield stress and the constitutive flow response at small strains, but it is sensitive to material imperfections/flaws over a large gauge area and is susceptible to failure at small strains on the order of the uniform elongation value in a tension test. For fresh cladding material, the plane-strain tension test is specifically designed to determine fracture behavior, and with proper experimental measurements, it is capable of establishing both a local and far-field fracture strain values in a stress state close to that of RIA conditions, albeit within a relatively small gauge area. The magneto-forming procedure progresses through a range of strain paths (and through-thickness strain gradients) that end up with strong biaxial nature on the cladding surface similar to that of cladding during a RIA. While still under development, it has the potential to generate difficult-to-measure failure strain data, but it is also limited to a small surface area of the cladding, and it would be difficult to implement in a hot cell to test irradiated material. Finally, in creating a small local region of plane-strain tension on the surface of the specimen under a condition of large through-thickness strain gradient, the ring compression test is well suited to establish fracture initiation conditions.

From the standpoint of determining the constitutive stress-strain response of the cladding, the ring tensile testing remains the basis for obtaining the constitutive flow behavior of high burnup cladding. The analysis requires finite element modeling and an assumption of the friction coefficient between the specimen and specimen grip/fixtures. Application of these data to deformation during RIA is then relatively straight-forward assuming a yield condition that may or not may take into account the low level of plastic anisotropy expected of the irradiated cladding [44]. Accurate determination of the constitutive flow behavior from expansion due to compression tests relies on finite elements analyses in which several friction issues need to be resolved, and for which studies are currently underway.

Finally, none of the tests described in this review address the issue of cladding failure in presence of a surface crack, such as might initiate due to a brittle hydride blister or heavily hydrided rim. In such a case, fracture initiation occurs in the form of a surface crack at negligible or very small plastic strains and cladding behavior is then dictated by the fracture mechanics associated with the growth of a through-thickness crack. Some recent crack-growth studies on un-irradiated Zircaloy-4 cladding provide preliminary data [32], but to our knowledge there is no current test procedure to address this issue for irradiated cladding.

6. Summary

Recent developments in the experimental procedures that address cladding failure behavior during a RIA are reviewed. An analysis of cladding strain data from RIA integral tests of rodlets in experimental reactors shows that the range of strain states during the RIA is comprised between plane-strain and equal-biaxial loading conditions. Thus, cladding failure occurs under multiaxial stress states even though the local strain path can be rather complex and depends on the degree of bonding between the fuel and the cladding.

Predicting the mechanical response of the fuel cladding during the RIA requires both understanding the constitutive deformation behavior and identifying the failure criteria under the multiaxial loading conditions and at the failure temperature. A brief review

of literature shows that failure strains of hydrided Zircaloy are indeed sensitive to both the multiaxial stress state and to the test temperature. The degree of sensitivity depends of hydride microstructure and mode of failure (i.e., whether or not crack initiation/growth control failure). Thus, accurate predictions of the deformation/failure behavior of fuel cladding during the RIA must account for several factors that must include (a) the range of stress states imposed on the cladding during RIA, (b) the mode of failure and associated failure criteria, and (c) the influence of temperature. As a consequence, data such as those in [16] should not be used for correction factors in predicting an RIA. Finally, although the anticipated strain rates are not exceedingly high ($\leq 5\text{ s}^{-1}$), strain rate may also affect failure, especially at elevated temperatures.

Current hoop tensile test procedures applicable to both irradiated tube material and separate effects tests are reviewed with respect to their ability to obtain (a) the appropriate deformation response and (b) importantly, the prototypical multiaxial stress states and failure modes of the RIA. Two main groups of hoop tensile tests currently exist: tests inducing an axial contraction within the specimen gage section such that a near-uniaxial tension stress state exists and tests characterized by multiaxial stress states within the gage section. The second group of tests has the potential of establishing failure conditions close enough to the RIA stress state such that only small stress-state corrections are needed. Although its strain path is not close to that of the RIA, the uniaxial ring tensile test (with its rather well-defined stress and strain states) remains the preferred procedure to establish the stress-strain response of the cladding with an acceptable accuracy.

It is concluded that careful analysis of the testing of irradiated materials and of separate effects tests is necessary to relate these results to integral tests and to assess the RIA behavior high burnup cladding. It is hoped that the current work provides an initial guide to the issues related to such an analysis.

Acknowledgments

The authors would like to thank many colleagues who contributed to develop the testing techniques addressed in the present paper, among them: Mike Billone, Robert Daum, Robert Montgomery, Kirill Lioutov, Slava Grigoriev, Tomoyuki Sugiyama, Aurore Parrot, Todd Link, Andrew Glendening, Olivier Pierron, Christian Bernaudat, Pascal Yvon, Christophe Poussard, Patrick Raynaud, Sébastien Carassou, Vincent Busser. The authors also thank the two anonymous reviewers who through their excellent reviews significantly improved the quality of this paper. Arthur Motta and Donald Koss are grateful for the support received for writing this paper from Harold Scott and the NRC.

References

- [1] P.E. MacDonald, S.L. Seiffert, Z.R. Martinson, R.K. McCardell, D.E. Owen, S.K. Fukuda, Nucl. Safety 21 (1980) 582–602.
- [2] R.O. Meyer, R.K. McCardell, H.M. Chung, D.J. Diamond, H.H. Scott, Nucl. Safety 37 (1996) 372–387.
- [3] R.S. Daum, S. Majumdar, H. Tsai, T.S. Bray, D.A. Koss, A.T. Motta, and, M.C. Billone, Mechanical Property Testing of Irradiated Zircaloy Cladding Under Reactor Transient Conditions, in: Proc. 4th Int. Sym. on Small Specimen Test Techniques, ASTM, STP 1418, 2002, pp. 195–210.
- [4] J. Papin, M. Balourdet, F. Lemoine, F. Lamare, J.M. Frizonnet, F. Schmitz, Nucl. Safety 37 (1996) 289–327.
- [5] V. Asmolov, L. Yegorova, Nucl. Safety 37 (1996) 343–371.
- [6] F. Schmitz, J. Papin, J. Nucl. Mater. 270 (1999) 55–64.
- [7] R.S. Daum, S. Majumdar, D.W. Bates, A.T. Motta, D.A. Koss, M.C. Billone, On the embrittlement of Zircaloy-4 under RIA-relevant conditions, in: Zirconium in the Nuclear Industry: Thirteenth International Symposium, ASTM STP 1423, 2002, pp. 702–718.
- [8] EPRI, Topical Report on Reactivity Initiated Accidents: Bases for RIA Fuel and Core Coolability, Palo Alto, CA, Doc. No. 2002.
- [9] R.O. Montgomery, Y.R. Rashid, O. Ozer, R.L. Yang, Nucl. Safety 37 (1996) 372–387.

- [10] V. Grigoriev, R. Jakobsson, D. Schrire, Further development of mechanical test simulate RIA in irradiated cladding, in: 24th NSRR Technical Review Meeting (JAERI-Conf 2001-010), Ibaraki-ken, Japan, JAERI, 2001, 139–49.
- [11] J. Desquines, B. Cazalis, C. Bernaudat, C. Poussard, X. Averty, P. Yvon, R. Daum, J. Rashid, D. Schrire, Mechanical properties of zircaloy-4 PWR fuel cladding with burnup 54–64MWd/kgU and implications for RIA behavior, in: 14th Symposium on Zr in the Nuclear Industry, Stockholm, Sweden, American Society for Testing and Materials (ASTM), STP 1467, 2005, pp. 851–872.
- [12] B. Cazalis, J. Desquines, C. Poussard, M. Petit, Y. Monerie, C. Bernaudat, P. Yvon, X. Averty, Nucl. Technol. 157 (2007) 215–229.
- [13] J. Papin, B. Cazalis, J.M. Frizonnet, J. Desquines, F. Lemoine, V. Georgenthum, F. Lamare, M. Petit, Nucl. Technol. 157 (2007) 230–250.
- [14] T. Nakamura, T. Fuketa, T. Sugiyama, H. Sasajima, J. Nucl. Sci. Technol. 41 (2004) 37–43.
- [15] F. Nagase, T. Fuketa, J. Nucl. Sci. Technol. 42 (2005) 58–65.
- [16] F. Yunchang, D.A. Koss, Metall. Trans. A 16A (1985) 675–681.
- [17] F. Prat, M. Grange, J. Besson, E. Andrieu, Metall. Mater. Trans. A 29A (1998) 1643–1651.
- [18] A. Glendening, D.A. Koss, A.T. Motta, O.N. Pierron, R.S. Daum, J. ASTM Int. 2 (2005) 1–16.
- [19] R. Manzel, M. Coquerelle, M.R. Billaux, Fuel Rod Behaviour at Extended Burnup, La Grange Park, IL, USA, ANS, 1994, 335–42.
- [20] K. Nogita, K. Une, J. Nucl. Sci. Technol. 34 (1997) 679–686.
- [21] H. Matzke, J. Spino, J. Nucl. Mater. 248 (1997) 170–179.
- [22] T. Fuketa, T. Nakamura and K. Ishijima, The status of the RIA test program in the NSRR, in: Proceedings of the Twenty-Fifth Water Reactor Safety Information Meeting, Bethesda, Maryland, NRC NUREG Report CP-01612, 2, 1997.
- [23] R.S. Daum, D.W. Bates, D.A. Koss, A.T. Motta, The influence of a hydrided layer on the fracture of Zircaloy-4 cladding tubes, in: International Conference on Hydrogen Effects on Material Behaviour and Corrosion Deformation Interactions, September 22–26, 2002, Moran, WY, United States, Minerals, Metals and Materials Society, Warrendale, PA 15086, United States, 2003, 249–258, BN-0873395018.
- [24] T. Fuketa, F. Nagase, K. Ishijima, T. Fujishiro, Nucl. Safety 37 (1996) 328–342.
- [25] K. Ishijima, T. Fuketa, Progress of the RIA experiments with high burnup fuels and their evaluation in JAERI, in: Proceedings of the Twenty-fourth Water Reactor Safety Information Meeting, Bethesda, Maryland, NRC NUREG Report CP-0157, 1, 1996.
- [26] T. Fuketa, H. Sasajima, T. Sugiyama, Nucl. Technol. 133 (2000) 50–62.
- [27] T. Fuketa, F. Nagase, T. Nakamura, H. Sasajima, H. Uetsuka, JAERI Research on fuel rod behavior during accident conditions, in: Proceedings of the Twenty-Seventh Water Reactor Safety Information Meeting, Bethesda, Maryland, NRC NUREG Report, vol. 2- CP-0169, 1999.
- [28] C. Bernaudat, S. Cambier, J. Guion, S. Benjamin, An analytical criterion to prevent PCMI fuel rod cladding failure during RIA transients, Light Water Reactor Fuel Performance Meeting, Paris, 2009.
- [29] A.T. Motta, A review of the critical strain energy density (CSED) model to analyzing reactivity initiated accidents (RIA) in high burnup fuel, NRC, Doc. No ML041030260, 2004. <<http://adamswbsearch.nrc.gov/idmws/ViewDocByAccession.asp?AccessionNumber=ML041030260>>.
- [30] F. Yunchang, PhD Thesis in Materials Science, Michigan Tech., 1985.
- [31] O.N. Pierron, D.A. Koss, A.T. Motta, K.S. Chan, J. Nucl. Mater. 322 (2003) 21–35.
- [32] A. Glendening, D.A. Koss, O.N. Pierron, A.T. Motta, R.S. Daum, J. ASTM Int. 2 (2005). paper ID12441.
- [33] P.R. Raynaud, A. Motta, D.A. Koss, K.S. Chan, Fracture toughness of hydrided zircaloy-4 sheet under through-thickness crack growth conditions, in: 15th International Symposium on Zr in the Nuclear Industry, Sunriver OR, ASTM, STP 1505, 2007, pp. 163–177.
- [34] T.M. Link, D.A. Koss, A.T. Motta, Metall. Mater. Trans. 31A (2000) 1883–1886.
- [35] M. Le Saux, J. Besson, S. Carassou, C. Poussard, X. Averty, Eng. Fail. Anal. 17 (2010) 683–700.
- [36] Cast3M web site. <<http://www-cast3m.cea.fr/cast3m/index.jsp>>
- [37] A. Hermann, S.K. Yagnik, D. Gavillet, Effect of local hydride accumulations on zircaloy cladding mechanical properties, Sunriver, OR, United states, American Society for Testing and Materials, 1505 STP, 2009, pp. 141–162.
- [38] A.M. Garde, G.P. Smith, R.C. Pirek, Effects of hydride precipitate localization on the ductility of irradiated zircaloy-4, in: 11th International Symposium on Zr in the Nuclear Industry, Garmisch-Partenkirchen, Germany, ASTM, STP 1295, 1996, 407–430.
- [39] L.M. Lowry, A.J. Markworth, J.S. Perrin, M.P. Landow, Evaluating strength and ductility of irradiated Zircaloy-4 Task 5, NRC, Doc.No NUREG/CR-1729, 1981.
- [40] L. Yegorova, V. Asmolov, G. Abyshov, V. Malofeev, A. vvakumov, E. Kaplar, K. Lioutov, A. Shestopalov, A. Bortash, L. Maiorov, K. Mikitiouk, V. Povlanov, V. Smirnov, A. Goryachev, V. Prokhorov, V. Pakhnitz, A. Vurim, Data base on the behavior of high burnup fuel rods with Zr-1%Nb cladding and UO₂ fuel (VVER type) under reactivity accident conditions, NRC, Doc.No NUREG/IA/0156 – vol. 2, 1999.
- [41] K.W. Barlow, R. Chandra, Int. J. Fatigue 27 (2005) 1661–1668.
- [42] J. Calcaterra, Samir Naboulsi, Int. J. Fatigue 27 (2005) 1133–1141.
- [43] S. Arsène, J. Bai, J. Test. Eval. 26 (1998) 26–30.
- [44] M. Le Saux, J. Besson, S. Carassou, C. Poussard, X. Averty, J. Nucl. Mater. 378 (2008) 60–69.
- [45] S. Arsene, J. Bai, P. Bompard, Metall. Mater. Trans. A (Phys. Metall. Mater. Sci.) 34A (2003) 579–588.
- [46] M. Veleva, S. Arsene, M.C. Record, J.L. Bechade, B. Jinbo, Metall. Mater. Trans. A (Phys. Metall. Mater. Sci.) 34A (2003) 567–578.
- [47] S. Arsene, J.B. Bai, P. Bompard, Metall. Mater. Trans. A (Phys. Metall. Mater. Sci.) 34A (2003) 553–566.
- [48] V. Grigoriev, R. Jakobsson, D. Schrire, Temperature Effect on BWR Cladding Failure Under Mechanically Simulated RIA Conditions, JAERI, Ibaraki-ken, Japan, 2002, 97–106.
- [49] O. Dufourneaud, A.G. Varias, V. Grigoriev, R. Jakobsson, D. Schrire, Numerical Simulation of the Expansion-Due-to-Compression Test, JAERI, Ibaraki-ken, Japan, 2002, 142–62.
- [50] T. Sugiyama, High burnup LWR fuel behavior under RIA conditions, Fuel Safety Research Meeting, Kyoto, Japan, October 7, 2005.
- [51] M. Le Saux, C. Poussard, X. Averty, C.S. Catherine, S. Carassou, J. Besson, High Temperature Expansion due to Compression Test for the Determination of a Cladding Material Failure Criterion under RIA Loading Conditions, American Nuclear Society, San Francisco, CA, United states, 2007, 526–535.
- [52] V. Grigoriev, R. Jacobson, D. Schrire, Hydrogen, burnup and temperature effects on bwr cladding failure under mechanically simulated RIA conditions, Poster presentation at the 14-th International Symposium on Zirconium in the Nuclear Industry, June 13–17, 2004, Stockholm, Sweden.
- [53] Vincent Busser, Marie-Christine, Baietto-Dubourg, Jean Desquines, Christian Duriez, Jean-Paul Mardon, J. Nucl. Mater. 384 (2) (2009) 87–95. 15 February.
- [54] T.M. Link, D.A. Koss, A.T. Motta, Nucl. Eng. Des. 186 (1998) 379–394.
- [55] S.L. Kampe, D.A. Koss, Acta Metall. 34 (1986) 55–61.
- [56] R.H. Wagoner, Metall. Mater. Trans. A 11A (1980) 165–175.
- [57] S. Carassou, M. Le Saux, J.P. Pizzanelli, O. Rabouille, X. Averty, C. Poussard, B. Cazalis, J. Desquines, C. Bernaudat, Ductility and Failure Behaviour of both Unirradiated and Irradiated Zircaloy 4 Cladding Using Plane Strain Tensile Specimens, Paris, France, 2009.
- [58] M. Leroy, A. Parrot, S. Leclercq, Failure characteristics of cladding tubes under RIA conditions through electromagnetic forming, SMIRT 19, Toronto, Canada, 2007.
- [59] S. Leclercq, A. Parrot, M. Leroy, Nucl. Eng. Des. 238 (2008) 2206–2218.